Structures 80 (2025) 109798

Contents lists available at ScienceDirect

Structures

journal homepage: www.elsevier.com/locate/structures

FEM-based practical recommendations for detailing UHPC wet joints of precast slabs

Marcos Antonio do Rosario da Silva [a], Alex Micael Dantas de Sousa [b,*], Daniel de Lima Araújo [c], Rafael Andrés Sanabria Díaz [d], Pablo Augusto Krahl [e], Mounir Khalil El Debs [a]

[a] University of São Paulo, São Carlos School of Engineering, São Carlos, Brazil
[b] São Paulo State University (Unesp), School of Engineering, Ilha Solteira, Brazil
[c] Federal University of Goiás, School of Civil and Environmental Engineering, Goiânia, Brazil
[d] Delft University of Technology, Delft, the Netherlands
[e] Mackenzie Presbyterian University, Science and Technology Center, Campinas, Brazil

ARTICLE INFO

Keywords:
Full-depth precast slab
Connection
UHPC
Numerical simulation
Wet joint detailing

ABSTRACT

The structural performance of bridges with full-depth precast slabs relies on the effectiveness of cast-in-place concrete wet joint in transferring forces. These wet joints are formed over interlocking reinforcement bars, with wet joint detailing being a critical factor in the behavior of slab connections. The reinforcement arrangement should be simple to manufacture, easy to assemble on-site, and ensure the durability and strength of the connection, which can be optimized by using ultra-high-performance fiber-reinforced concrete (UHPC). This study investigates the performance of different reinforcement wet joint configurations in connections between full-depth precast slabs and evaluates their performance using UHPC as wet joint filler material. Experimental results were selected from the literature to calibrate the behavior of finite element model of the wet joint. Numerical results showed that the UHPC properties contribute significantly to enhance connection performance, particularly in the anchorage between reinforcement bars, allowing for reduced reinforcement splice length compared to conventional concrete. Anchorage failure is avoided with a minimum connection length of 200 mm and a splice length of at least 7.5 times the diameter of the longitudinal bars (d_b). Additionally, the use of headed or looped bars in the connection improves reinforcement anchorage.

1. Introduction

The use of full-depth precast concrete slabs in bridge decks has grown in recent decades due to their advantages over cast-in-place concrete slabs, such as (i) faster building speed, (ii) greater quality control of structural elements, (iii) reduced impact on traffic, (iv) more rational use of natural resources (sustainability) and (v) minimization of environmental disturbances [1]. In the case of bridge superstructure composed of precast beams and pre-slabs (Fig. 1a), the volume of cast-in-place concrete (CIP) is still relatively high. Aiming to reduce CIP consumption and, mainly, construction time, other systems have grown around the world based on the combination of precast elements, such as full precast slabs and beams with integrated slabs (bulb tee girders - Fig. 1b). However, the performance of this type of system depends mainly on the design and detailing of the connection region between these elements.

Generally, connections using interlocking reinforcement filled with cast-in-place concrete are adopted between precast elements. An example of a connection between full-depth precast slabs is shown in Fig. 2. According to Wang et al. [2], the bearing capacity of these connections is influenced by design variables such as the geometric details of the connection, the properties of the concrete as a filler material, and the reinforcement joint/anchorage configuration.

Ultra-high-performance fiber-reinforced concrete (UHPC) has emerged as an interesting option to fill these connections and for improving bridge resilience [4]. It presents characteristics such as higher tensile/crack resistance and better adhesion to the precast slab [5–7]. Besides, Haber and Graybeal [8] performed static and fatigue tests on reduced models of precast bridge decks connected by UHPC connections. The results showed that, due to the higher adhesion

* Corresponding author.
E-mail address: alex.dantas@unesp.br (A.M.D. de Sousa).

https://doi.org/10.1016/j.istruc.2025.109798
Received 9 June 2025; Received in revised form 11 July 2025; Accepted 22 July 2025
Available online 26 July 2025

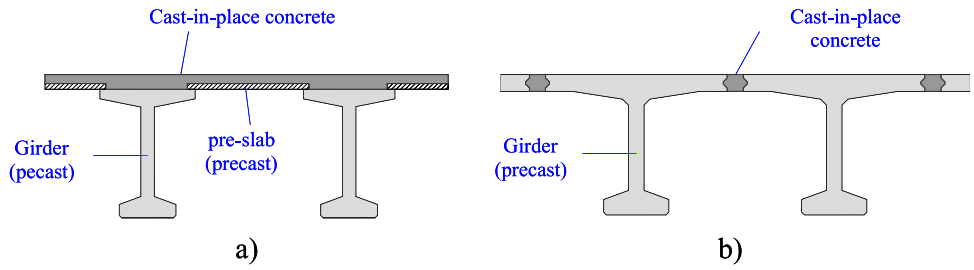

Fig. 1. a) Cast-in-place concrete for a) precast slabs between girders and b) full-depth precast slabs (bulb tee girders).

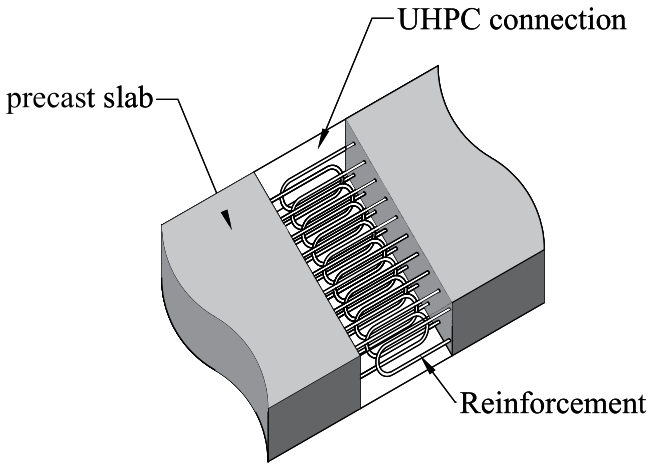

Fig. 2. Example of connection between full precast bridge slabs [3].

strength of UHPC with hardened concrete, failures occurred mainly in the precast slabs, while the UHPC connections remained intact during the loading process.

The inclusion of fibers in UHPC also improves the adhesion of the reinforcement to the concrete in the connection. Steel fibers uniformly distributed in the matrix improve tensile properties [9]. The use of UHPC in connections allows reduction of connection widths and minimized cracking at the interface [3].

One of the most critical factors influencing the load-bearing capacity of connection between precast elements is the detailing of reinforcement splices. The ideal reinforcement arrangement should be easy to manufacture, simple to assemble on-site, and ensure both durability and structural strength [1]. Typically, non-contact lap-spliced reinforcement bars are used with different detailing approaches. Among the various splice types, the most commonly employed is the straight bar splice, where bars are connected through lap splicing [2]. In this configuration, reinforcement anchorage is achieved through the bond between the bars and the connection's concrete. However, straight bars require a long splice length to ensure adequate anchorage, which can be impractical in bridge deck design.

To address this challenge, researchers have explored different reinforcement detailing methods to reduce the lap splice length and, consequently, the overall connection length. One alternative to straight bars in connections is the use of headed bars, which rely on mechanical anchorage [10]. In this system, stress transfer occurs primarily between overlapping headed bars through a series of diagonal compression struts.

Another alternative is the use of U-shaped (looped) bars [11]. In this configuration, the bars are bent at 180°, enabling tensile force transfer from the U-bar to the connection's concrete, thereby enhancing mechanical anchorage. As a result, this approach allows for a reduction in the overall connection length.

According to Hussein et al. [12], bridge structures, frequently subjected to traffic loads and environmental actions, experience shear, tension, compression, and bending moments that act on these connections. When the primary force transferred between slabs is bending moment, three possible failure mechanisms can occur in this type of connection: (i) yielding of the longitudinal reinforcement; (ii) concrete crushing; and (iii) failure of the reinforcement splice.

The yielding of longitudinal reinforcement determines the flexural strength of the deck connection. Although concrete crushing is the most critical failure mode due to its brittle nature, it can generally be prevented through conventional flexural design principles.

Failure around the longitudinal reinforcement splices can occur due to reinforcement slippage within the connection's concrete once the bond stress reaches its limit. Anchorage failure often results from insufficient lap splice length, frequently leading to the detachment of the concrete cover along the longitudinal reinforcement. For this reason, ensuring proper reinforcement splicing is the most crucial aspect of this type of connection.

2. Research significance

Despite the increasing number of studies on the behavior of full-depth precast panels using UHPC as filling cast-in-place material, some limitations can be identified. For instance, the joint width is frequently large enough to avoid any anchorage failure [8]. In this way, it is unknown how large the ratio between the joint width that could trigger the anchorage failure and the one that would be sufficient to promote a ductile flexural failure mechanism. Despite that, several numerical studies have been published considering a perfect bond between the reinforcement and the surrounding concrete [13–15] which can limit the reliability of the results. In other words, no anchorage failure could be identified using such a modeling approach, which introduces a bias in the presented results since any tested detailing option would appear as sufficient to avoid anchorage failure. Therefore, a parametric study was developed based on a detailed consideration of the bond-slip properties between the reinforcement and UHPC, providing practical recommendations for the design of UHPC cast-in-place joints. In summary, this study proposes a framework for non-linear finite element analyses that allows for the proper investigation of the influence of different reinforcement detailing options on the behavior of full-depth precast joints filled with UHPC. In other words, the proposed approach includes recommendations on the bond-slip relationships that should be considered to simulate anchorage failure for such joints when using limited-width connections.

3. Material modeling

3.1. Concrete

The Total Strain Constitutive Model was employed for both normal strength concrete (NSC) and Ultra-High-Performance Concrete (UHPC), based on the Modified Compression Field Theory developed by Vecchio and Collins [16] and later modified by Selby and Vecchio [17]. The properties of NSC were utilized for the precast panels, while UHPC was

Table 1
Constitutive model of NSC.

Parameter	Description
Cracking model	Total strain fixed crack
Tensile stress-crack opening behavior	Hordijk [18]
Tensile fracture energy (G_f)	*fib* Model Code 2010 [19]
Compression behavior	Parabolic model[20]
Compressive fracture energy (G_c)	250 G_f, Nakamura and Higai [21]

Table 2
Constitutive model of UHPC.

Parameter	Description
Cracking model	Total strain fixed crack
Tensile stress-crack opening behavior	Multilinear curve, Fehling et al. [22]
Compression behavior	Thorenfeldt et al. [23]

used for the wet joint. Table 1 and Table 2 provide the input parameters for the behavior of NSC and UHPC under both tension and compression, respectively.

The constitutive models adopted to represent the tensile behavior of NSC were the Hordijk model [18], and for UHPC, the model by Fehling et al. [22] was adopted. The curve proposed by Hordijk [18] establishes a linear-elastic relationship up to the point of maximum tensile strength, and after cracking, a constitutive law based on fracture energy relates the normal tensile stress (f_t) to the normal strain to the crack (ε) that is used to describe the softening of concrete. The fracture energy (G_f) is defined as the amount of energy required to propagate a unit surface crack. The tensile behavior curve proposed by Hordijk [18] is described by the equation below.

$$\frac{\sigma(\varepsilon)}{f_t} = \left(1 + c_1 \frac{\varepsilon}{\varepsilon_{ult}}\right) e^{-c_2 \frac{\varepsilon}{\varepsilon_{ult}}} - \frac{\varepsilon}{\varepsilon_{ult}}\left(1 + {c_1}^3\right) e^{-c_2} \tag{1}$$

The values of the constants are $c_1 = 3$ and $c_2 = 6.93$ were used. The value of the ultimate deformation (ε_{ult}) corresponds to the crack opening in which the residual tensile strength is zero and is defined by:

$$\varepsilon_{ult} = 5.14 \frac{G_F}{h f_t} \tag{2}$$

In smeared crack models, the bandwidth value (h) defines the length over which the crack width, w, is distributed at each integration point of the element. This ensures that the cracking process is independent of the size of the finite element. The bandwidth value depends on the type of element, its size, and the integration points and is calculated automatically in the software.

The fracture energy value G_f is calculated from Eq. (3), defined by the *fib* Model Code 2010 [19]:

$$G_f = 73 {f_c}^{0.18} [N/mm] \tag{3}$$

In this study, the model by Fehling et al. [22] was applied to represent the tensile behavior of UHPC due to considering the effects of fibers in concrete. The formulation is based on the stress-crack width relationship according to Eq. (4).

$$f_t(w) = f_{ct}\left(1 - 2\frac{w}{l_f}\right)^2 \tag{4}$$

Where l_f is the length of the steel fibers (equal to 13 mm in the reference experimental program). The total tensile strain can be calculated based on the crack-opening from the following relationship:

$$\varepsilon_t = \frac{f_{ct}}{E_c} + \frac{w}{l_{eq}} = \varepsilon_{t,cr} + \frac{w}{l_{eq}} \tag{5}$$

Where l_{eq} is length related to the finite element size. The behavior of concrete under compression was simulated using the curve proposed by Feenstra [20] for NSC and Thorenfeldt et al. [23] for UHPC, respectively. Both models are available in DIANA FEA. The compression models were adopted because they best fit the results of the experimental model among the alternatives available in the software. The stress-strain behavior model proposed by Feenstra [20] is based on fracture energy and divides the behavior of concrete into three deformation values: $\varepsilon_c/3$ is the deformation at which one-third of the compressive strength is reached, ε_c is the deformation at which the compressive stress is equal to the compressive strength and ε_u is the ultimate deformation at which the concrete softens completely. These values were calculated by equation (6).

$$\varepsilon_{c/3} = -\frac{1}{3}\frac{f_c}{E_c} \tag{6a}$$

$$\varepsilon_c = -\frac{5}{3}\frac{f_c}{E} \tag{6b}$$

$$\varepsilon_u = \varepsilon_c - \frac{3}{2}\frac{G_c}{h f_c} \tag{6c}$$

The parabolic curve is therefore described as by Eq. (7):

$$\sigma(\varepsilon) = \begin{cases} -\frac{1}{3}\frac{f_c \varepsilon}{\varepsilon_{c/3}} \text{se} \varepsilon_{c/3} < \varepsilon \leq 0 \\ -\frac{f_c}{3}\left[1 + 4\left(\frac{\varepsilon - \varepsilon_{c/3}}{\varepsilon_c - \varepsilon_{c/3}}\right)\right] - 2\left(\frac{\varepsilon - \varepsilon_{c/3}}{\varepsilon_c - \varepsilon_{c/3}}\right)^2 \text{se} \varepsilon_c < \varepsilon \leq \varepsilon_{c/3} \\ -f_c\left[1 - \left(\frac{\varepsilon - \varepsilon_{c/3}}{\varepsilon_c - \varepsilon_{c/3}}\right)^2\right]^2 \text{se} \varepsilon_u < \varepsilon \leq \varepsilon_c \\ 0 \text{se} \varepsilon_u < \varepsilon \leq \varepsilon_u \end{cases} \tag{7}$$

The concrete softening in compression is dependent on the crushing energy G_c and the finite element bandwidth of h. According to Nakamura and Higai [21] the crushing energy G_c can be estimated as 250 times the tensile fracture energy G_f.

The stress-strain behavior model in compression proposed by Thorenfeldt et al. [23] is described by the Eq. (8):

$$\sigma(\varepsilon) = f_c \frac{\varepsilon}{\varepsilon_c}\left[\frac{n}{n - \left(1 - \left(\frac{\varepsilon}{\varepsilon_c}\right)^{nk}\right)}\right] \tag{8}$$

Where f_c is the compressive strength; ε_c is the compressive strain corresponding to the compressive strength; the constants n and k are defined as:

$$n = 0.80\frac{f_c}{17} \;;\; k = \begin{cases} 1 \text{se} \varepsilon_c < \varepsilon \leq 0 \\ 0.067 + \frac{f_c}{62} \text{se} \varepsilon \leq \varepsilon_c \end{cases} \tag{9}$$

3.2. Steel

The constitutive model adopted for the reinforcements was the elastoplastic model with von Mises plasticity criteria. The elastoplastic model with linear hardening was considered. Bond-slip relationship between the reinforcement and the surrounding concrete was assumed, as explained in the next item.

3.3. Bond-slip modeling

Slipping between the steel bars and the concrete is fundamental in several structural situations of reinforced concrete, such as checking for possible anchorage failures due to insufficient overlap length [24]. In numerical simulations, the mechanical behavior of slippage can be simulated through zero-thickness interface elements. In this study, the model presented by *fib* Model Code 2010 [19] was considered for the longitudinal bars located in the region of the normal strength concrete

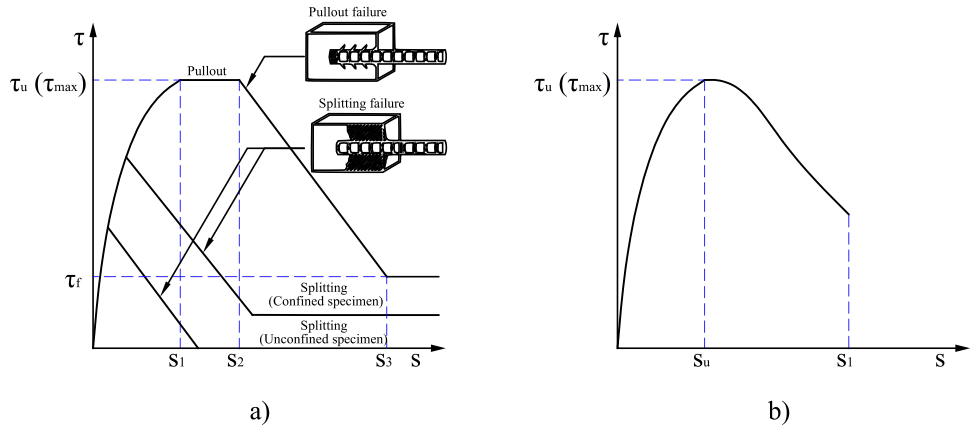

Fig. 3. a) Bond-slip stress model considered for a) NSC according to the Model Code 2010 and b) for UHPC according to Pan et al. [25].

Table 3
Parameters for defining the bond-slip relationship of NSC according to *fib* Model Code 2010.

	1	2	3	4	5	6
	Pull-Out		**Splitting**			
	$\varepsilon_s<\varepsilon_{s,y}$		$\varepsilon_s<\varepsilon_{s,y}$			
	Good bond cond.	All other bond cond.	Good bond cond.		All other bond cond	
			unconfined	stirrups	unconfined	stirrups
τ_u	$2.5\sqrt{f_c}$	$1.25\sqrt{f_c}$	$7.0\left(\frac{f_c}{20}\right)^{0.25}$	$8.0\left(\frac{f_c}{20}\right)^{0.25}$	$5.0\left(\frac{f_c}{20}\right)^{0.25}$	$5.5\left(\frac{f_c}{20}\right)^{0.25}$
s_1	1.0 mm	1.8 mm	$s(\tau_u)$	$s(\tau_u)$	$s(\tau_u)$	$s(\tau_u)$
s_2	2.0 mm	3.6 mm	s_1	s_1	s_1	s_1
s_3	c_{clear}	c_{clear}	1.2 s_1	$0.5c_{clear}$	1.2 s_1	$0.5c_{clear}$
A	0.4	0.4	0.4	0.4	0.4	0.4
τ_f	$0.4\tau_u$	$0.4\tau_u$	0	$0.4\tau_u$	0	$0.4\tau_u$

Where c_{clear} is the clear distance between ribs.

used in the precast panels (Fig. 3a).

The parameters for defining the bond-slip properties from NSC are presented in Table 3. In this simulation, the splitting failure model was considered due to insufficient concrete cover, smaller than $5d_b$. For the flexural test, good bond conditions and confinement due to the existence of transverse reinforcement in the joint region were considered; from this, model 4 from Table 3 was chosen to determine the adhesion behavior.

The model chosen to represent the bond-slip behavior between the reinforcement and the UHPC is the one proposed by Pan et al. [25], Fig. 3b, because it presents better agreement with the experimental results. Furthermore, it considers the parameter of the embedment length of the bars in the concrete (l_e), which is one of the analysis objectives of this study.

$$\tau_u = k_f\sqrt{f_c}(0.426d_b - 0.954)\left(0.267\frac{d_b}{l_e} + 0.0913\frac{c}{d_b} + 0.162\right)$$

$$k_f = 0.6462 + 0.1033V_f \le 1$$

Where f_c is the compressive strength of the concrete; f_t is the tensile strength of the concrete; d_b is the rebar diameter; c is the concrete cover; l_e is the length of the bar embedded in the concrete; V_f is the volume of fibers; l_f is the fiber length; and d_f is the fiber diameter. The bond-slip model from Pan et al. [25] comprises an ascending section up to the maximum bond stress (τ_u) and a descending section, as seen in Fig. 3b. The ascending section of the curve ($0 < S < S_u$) includes the microslip stage and the interlocking friction slip stage, which is described by:

$$\tau = \tau_u\left(1 - e^{-\frac{S}{\alpha S_u}}\right)^{\beta} \tag{10}$$

where $\alpha = 0.263$ and $\beta = 1.213$. For the descending branch ($S_u < S < S_1$), the bond stress is calculated as:

$$\tau = \tau_u\left(1 - 0.252\left(\frac{S}{S_u} - 1\right) + 0.034\left(\frac{S}{S_u} - 1\right)^2 - 0.002\left(\frac{S}{S_u} - 1\right)^3\right) \tag{11}$$

The determination of the ultimate sliding S_u that corresponds to the maximum bonding stress for anchorage failure to occur is defined by:

$$s_u = 0.4w_r(1 + 0.5V_f)\left(0.293 + 0.056\frac{c}{d_b}\right) \tag{12}$$

Where w_r is the width of the ribs of the steel bar, which is considered for the simulation as equal to 4.8 mm; V_f is the fiber volume (2 %); c is the concrete cover, and d_b is the rebar diameter. The value adopted for the sliding S_1 is given by:

$$S_1 = 0.83S_r \tag{13}$$

In this simulation, s_r represents the spacing between the ribs of the rebar, which was set to 7.9 mm.

4. Validation of proposed modeling framework

In this section, the numerical modeling validation procedure is presented. First, pull-out tests on UHPC conducted by Soliman et al. [26] were used to validate the bond-slip model described in the previous

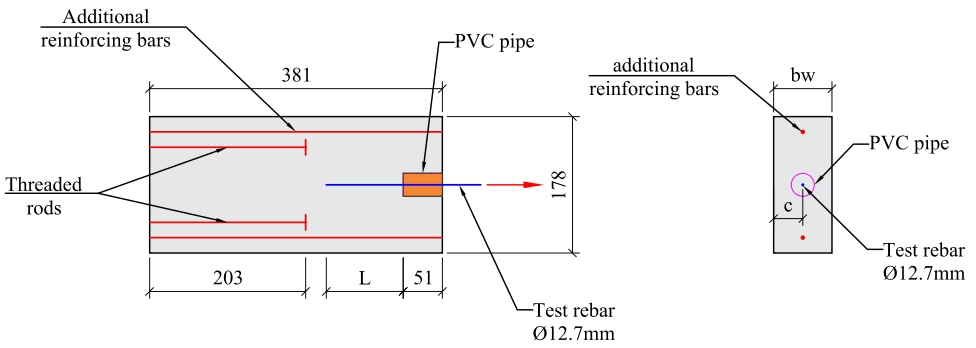

Fig. 4. Pull-out tests geometry (dimension in mm). Source: Adapted from Soliman et al. [26].

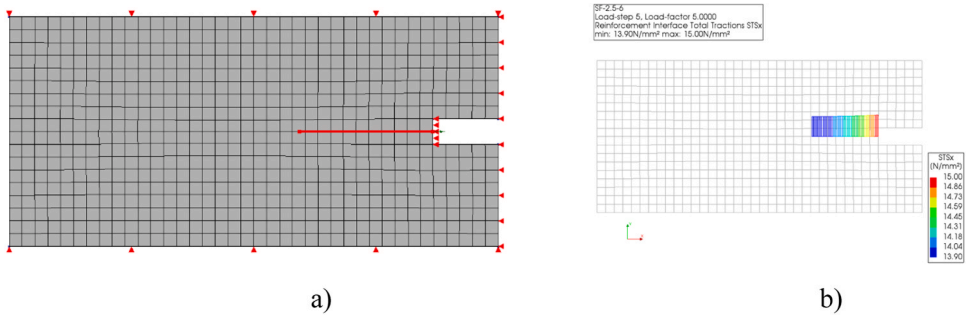

Fig. 5. a) Finite element model SF-2.5–6 with the respective boundary conditions and mesh discretization; and b) results of bond stress at the reinforcement in the test SF-2.5–6.

section. Subsequently, flexural tests on wet joints between precast slabs, performed by Deng et al. [27], were employed for further validation at the structural level.

4.1. Pull-out tests on UHPC

An accurate bond-slip constitutive model is crucial for representing possible anchorage failures due to insufficient overlapping length. Based on that, a specific evaluation of the bond-slip model considered was conducted using the simulation of pull-out tests.

To ensure the reliability of the numerical analysis, a calibration phase was performed to adjust the model parameters, enhancing the agreement between the numerical and experimental results. The bond-slip model proposed by Pan et al. [25] for UHPC-concrete interfaces was applied in the simulations, and its performance was validated through comparison with bar pull-out tests conducted by Soliman et al. [26]. The test details are presented in Fig. 4.

The UHPC compressive strength is 151.2 MPa, the tensile strength is 7.4 MPa, and the modulus of elasticity is 40 GPa. The yield strength and ultimate strength of the steel were 414 and 700 MPa, respectively, with a modulus of elasticity of 200 GPa. The specimen names were designated as follows: SF stands for straight steel fibers; followed by the cover thickness (c) and the embedded length of the reinforcement bar (L), both expressed as multiples of d, where d is the diameter of the bar (12.7 mm). For example, specimen SF-1.5–3 refers to a test using UHPC with straight steel fibers, a cover thickness of 1.5d, and an embedded bar length of 3d.

The numerical model was developed considering eight-node isoparametric quadrilateral plane stress elements (CQ16M). The load application was defined as a prescribed displacement of 0.1 mm across 50 steps, resulting in a total of 5 mm displacement. This 2D approach was chosen to validate the bond-slip model due to its lower computational cost and simplicity compared to full 3D simulations. It enables an efficient preliminary assessment of the bond behavior between the reinforcement and the surrounding concrete, ensuring that the constitutive model performs adequately under controlled conditions before being implemented in a more complex 3D finite element framework. In Fig. 5, the finite element model and the result of the reinforcement bar bond stresses are presented, respectively.

Fig. 6 shows the results of the pull-out force-slip curves of the numerical simulations and the experimental tests.

On average, the tests and numerical simulations agree well regarding the predicted force-slip curves (Shown in Table 4). A closer agreement is observed in specimens with greater embedment lengths suggesting that the numerical bond-slip model more accurately captures the load transfer behavior when the anchorage length is sufficient to distribute stresses more uniformly along the steel-concrete interface. In these cases, the bond mechanism is governed predominantly by adhesion and friction over a longer contact surface, reducing the influence of localized stress concentrations and premature debonding, which are more difficult to simulate accurately in shorter embedded lengths.

4.2. Bending panel with UHPC wet joint

Precast concrete slabs with UHPC connections subjected to flexure were tested in the experimental program developed by Deng et al. [27]. Seven slabs from this work were selected to calibrate the finite element model. These tests were chosen because they present different design configurations related to reinforcement ratio, overlapping form and length of reinforcement. Fig. 7 shows the different connection designed configurations used by Deng et al. [27].

The experimental program considered slabs with different connection design options such as (i) joint length per overlap, (ii) detailing of the type of reinforcement joint in the connection, and (iii) reinforcement ratio. The details of the models tested by Deng et al. [27] are described in Table 5.

Group A is a monolithic concrete slab without discontinuity of reinforcement used as a reference in the experimental program. Groups B, C, and D were designed to investigate the influence of joint detail and longitudinal reinforcement ratio on the flexural behavior of the UHPC

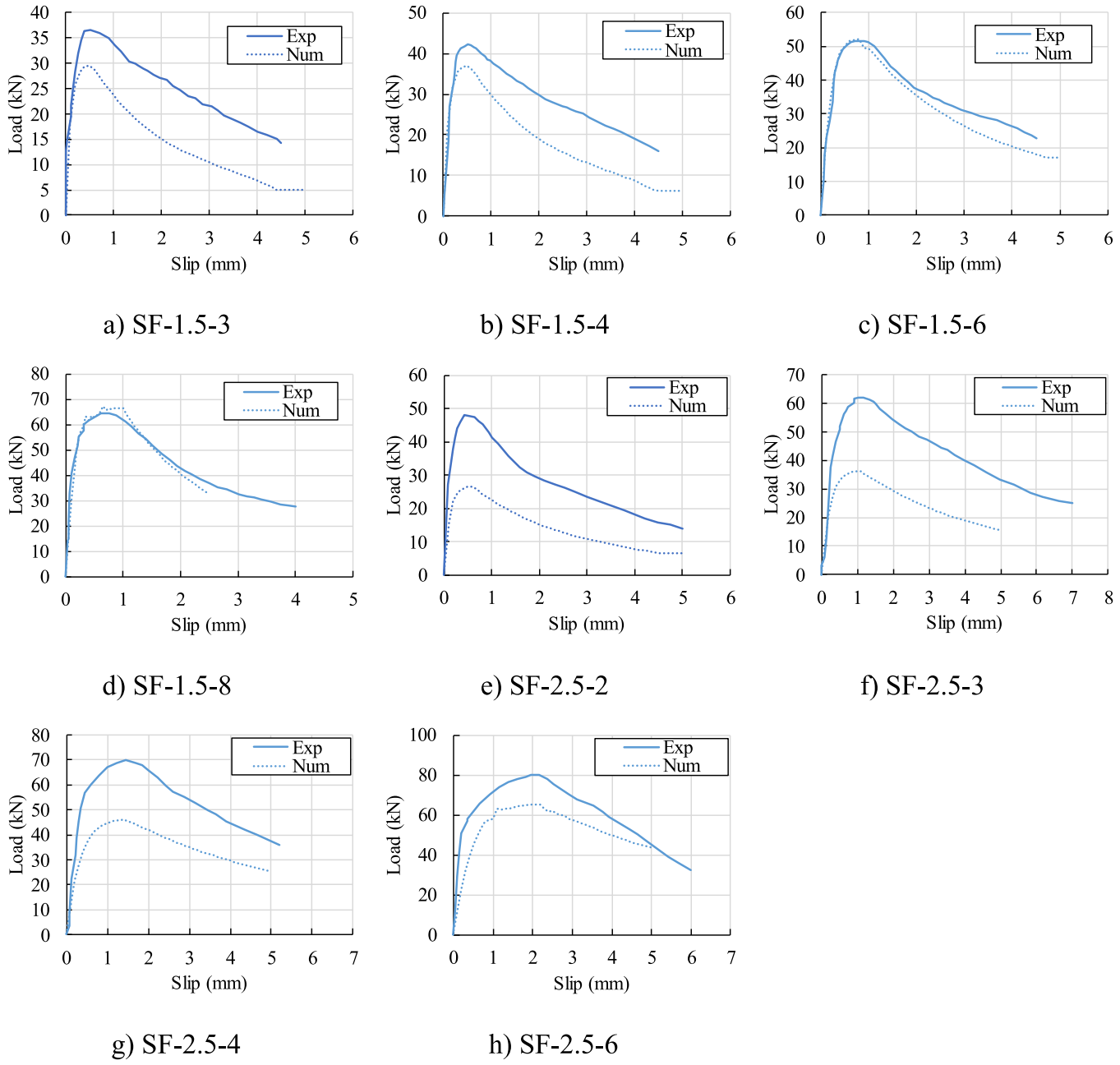

Fig. 6. Comparison between experimental and numerical results of the pull-out tests performed by Soliman et al. [26].

Table 4
Comparison of pull-out strength of experimental and numerical models.

Model	F_{exp}	F_{num}	F_{exp}/F_{num}
SF-1.5–3	36.56	29.53	**1.24**
SF-1.5–4	42.25	36.97	**1.14**
SF-1.5–6	51.53	52.28	**0.99**
SF-1.5–8	64.48	67.27	**0.96**
SF-2.5–2	48.06	26.54	**1.81**
SF-2.5–3	62.11	36.23	**1.71**
SF-2.5–4	69.95	46.02	**1.52**
SF-2.5–6	80.19	65.31	**1.23**
AVG			**1.32**
COV			**24.3 %**

connection, respectively.

The specimen's names were designated as follows: connection shape (R = rectangular); reinforcement splice detail (A = annular; S = Straight); reinforcement splice length – L (mm); reinforcement ratio (1.13 % or 1.35 %)". For instance, specimen RA-332–1.13 refers to the deck featuring a rectangular section form of the wet joint, along with longitudinal reinforcements that include annular-shaped overlap reinforcement, as illustrated in Fig. 2. Meanwhile, the flexural reinforcement ratio and the length of lap splice are 1.13 % and 332 mm, respectively.

All slabs are rectangular, with uniform dimensions of 2112 mm × 1000 mm and a thickness of 200 mm. The specimens featuring the UHPC connection consisted of two precast concrete panels (PCP), each measuring 850 mm × 1000 mm × 200 mm, with the connection measuring 412 mm in length. Four-point bending tests were carried out by Deng et al. to examine the bending moment behavior of the models. The details of this setup can be found in Fig. 8, which illustrates how the central section remains under a constant bending

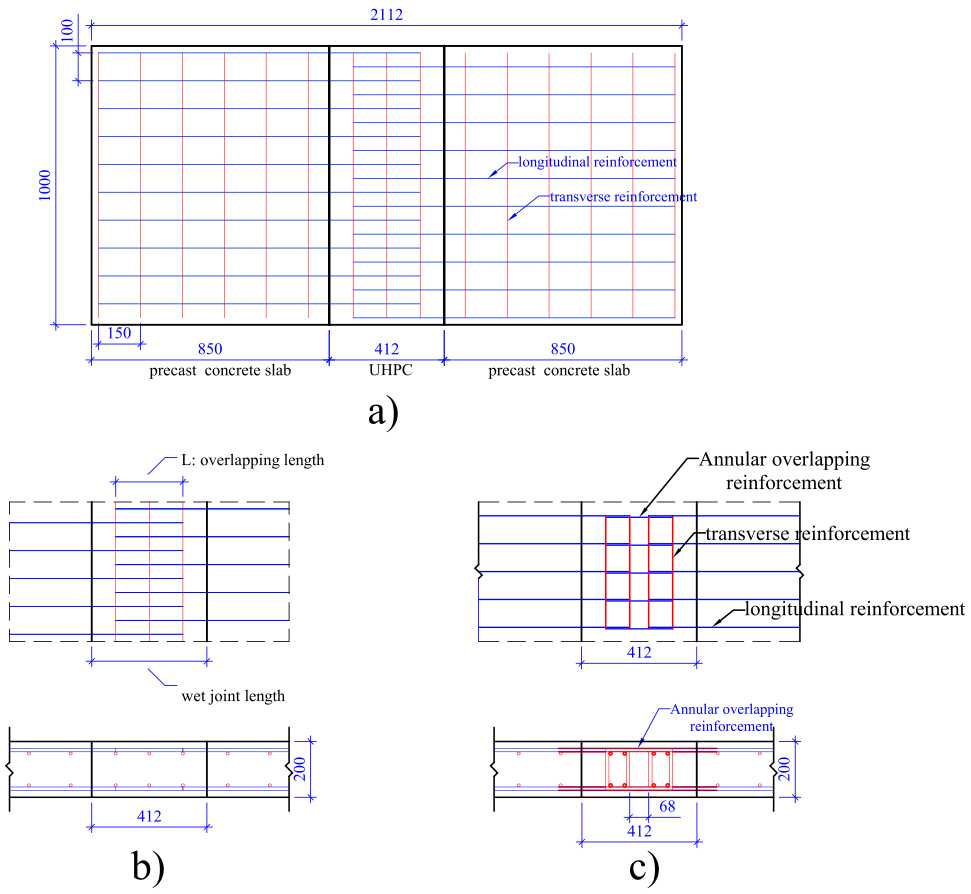

Fig. 7. Geometry of the tested slabs (dimensions in mm): a) Top view; b) cross-section view of the connection or wet joint with straight lap length or overlapping length; c) Annular overlapping of the reinforcement. Source: Adapted from Deng et al. [27].

Table 5
Parameters of the test specimens. Source: Adapted from Deng et al. [27].

Group	Specimen	ρ (%)	Overlapping form of reinforcement	Overlapping length L (mm)
A	ICBD	-	-	-
B	RA-332–1.13	1.13	Annular	332
	RA-354–1.13	1.13	Annular	354
C	RS-120–1.13	1.13	Straight	120
	RS-180–1.13	1.13	Straight	180
D	RS-120–1.35	1.35	Straight	120
	RS-240–1.35	1.35	Straight	240

moment.

The hydraulic mechanical actuator applies the two vertical loads close to the joint. The specimens were subjected to monotonic loading until the element failed. Table 6 describes the properties of the materials used in the experimental tests. For the precast concrete panels, the average compressive strength of the concrete was 52.2 MPa, and the tensile strength and modulus of elasticity were estimated with the expressions of the *fib* Model Code 2010 [19].

The average compressive strength f_{cm} and modulus of elasticity E_c of UHPC were 131.3 MPa and 41.4 GPa, respectively. Approximately 2.5 % by volume of straight steel fibers were used in the UHPC mixture. The tensile strength of UHPC was estimated from the recommendation of Fehling et al. [22] presented in Eq. (14).

$$f_{ct} = 0.3\sqrt[3]{f_{cm}{}^2} \tag{14}$$

The slab reinforcement consisted of HRB400 steel bars with a diameter (d_b) of 12 mm, arranged longitudinally and transversely. The concrete cover was 25 mm. A spacing of 150 mm was used for the transverse bars ($\rho_t = 0.8$ %) and 100 mm for the longitudinal bars ($\rho_l =$ 1.13 %), except for model D, which used a spacing of 80 mm for the longitudinal bars ($\rho_l = 1.35$ %). The yield stress of the reinforcement was 409.6 MPa.

In the loading simulation, incremental displacement was applied to represent the hydraulic actuator in the load application region. This approach allows for a better analysis of the structure's non-linear behavior after the post-peak load. In Fig. 9, vertical displacement is applied of the model using two rigid steel plates. Each plate is 100 mm wide and 20 mm thick. The displacement is applied in increments of 0.2 mm across 250 steps, resulting in a total of 50 mm displacement.

Rigid steel plates were considered for the two support points, with the displacement degrees of freedom in the x, y, and z directions restricted on the left side. Additionally, the displacement degrees of freedom in the y and z directions of the plate on the right side were also restricted to create a simple support boundary condition. The degrees of freedom for rotation were permitted to prevent stress concentrations at the support.

To represent experimental behavior more accurately, interface elements (CQ48I) were applied between the precast panels and the support and loading plates. These elements were also used at the interface between the precast panels and the UHPC.

For the input data of the interface between the support and loading plates and the panels, the normal stiffness of 0.4 N/mm^3 and tangential

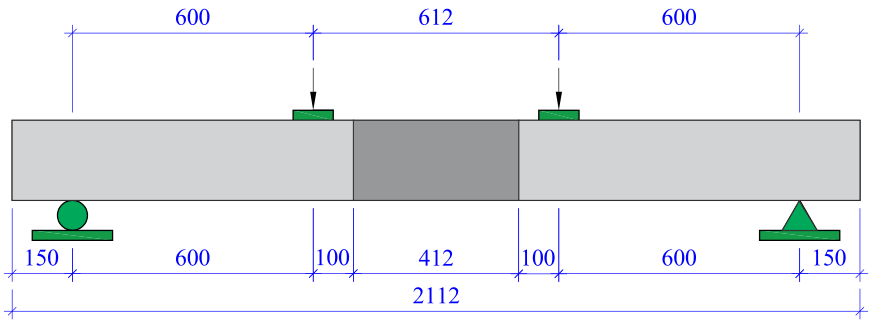

Fig. 8. Detail of the four-point bending test (dimensions in mm). Font: Adapted from Deng et al. [27].

Table 6
Material Properties. Font: Deng et al. [27].

Material	f_y (MPa)	f_u (MPa)	E_s (GPa)
Steel	409.6	552.9	205.8
	f_{cm} (MPa)	**f_{ct} (MPa)**	**E_c (GPa)**
PCP	52.2	4.2	37
UHPC	131.3	7.75	41.4

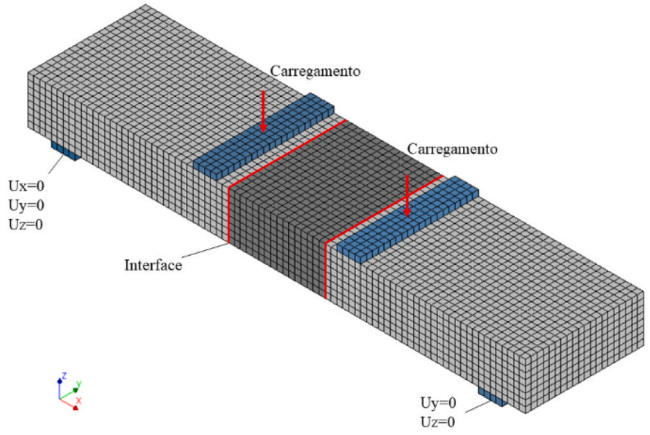

Fig. 9. Finite element mesh and boundary conditions.

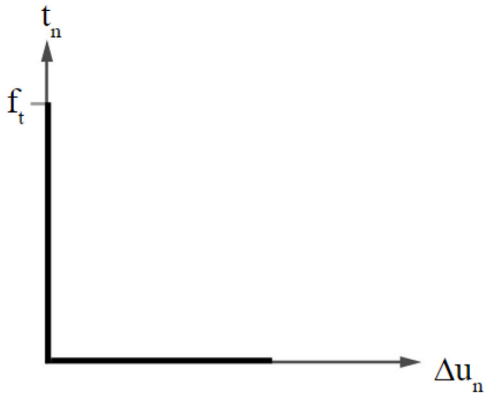

Fig. 10. Brittle cracking behavior. Font: DIANA FEA [28].

stiffness of 1.0 N/mm³ were considered, given the interface's non-linear behavior. These stiffness values were defined from the calibration with the experimental model to fit the force-displacement curves.

The interface between UHPC and conventional concrete was modeled using the discrete cracking interface model with a brittle cracking criterion, available in DIANA FEA [28]. This approach assumes a complete loss of tensile strength at the interface once the failure criterion is reached [28], shown in Fig. 10.

Table 7
Parameters for interface between UHPC and normal concrete.

Parameters	Adopted Value	Observations
Constitutive model	*Discrete Cracking*	Available in DIANA FEA
Normal stiffness (K_n)	241,4 N/mm³	Prado [29]
Tangential stiffness (K_t)	161,5 N/mm³	Prado [29]
Tensile strength ($f_{t,f}$)	4,2 MPa	Prado [29]
Tensile behavior	*Brittle Cracking*	Available in DIANA FEA
Shear behavior	*Zero shear traction*	Available in DIANA FEA

Brittle cracking behavior:

$$\frac{f_n(\Delta u_n)}{f_t} = \begin{cases} 1 \text{se} \Delta u_n \le 0 \\ 0 \text{se} 0 \le \Delta u_n \le \infty \end{cases} \quad (15)$$

Table 7 shows the input data of the interface parameters model between the normal concrete slabs and the UHPC connection. The interface characterization parameters used were obtained from the study by Prado [29] considering the treatment of the interface with exposed aggregates.

The solution method adopted was the secant, or Quasi-Newton method with BFGS formulation, where the tangent stiffness matrix is calculated using the secant direction between two previous consecutive solutions, thus allowing an update of the stiffness matrix in each iteration, with lower computational cost than the Newton-Raphson method. The slabs and plates were modeled using three-dimensional 8-node finite elements (CHX60), with a mesh density of 8 elements along the slab thickness and element dimensions of 25 × 25 × 25 mm.

This configuration provided good convergence behavior and reduced computational time without compromising the accuracy of the results. Fig. 11 shows a comparison between tested and numerical results in terms of the force−displacement at the midspan of the tested slabs.

It can be stated from Fig. 11 that the numerical models reproduced the flexural strength well. By observing the graphs, it can be stated that the mechanical performance of the models is divided into three stages: elastic stage, cracking stage, and yielding stage.

To better analyze the mechanical performance of the models, comparisons were made between the numerical and experimental results of the loads at the points of first cracking, steel yielding, and maximum capacity. The comparison of the load points and displacement ductility obtained experimentally and with the numerical models in finite elements is presented in Table 8.

The results indicate that the proposed modeling approach accurately predicted the flexural strength of the slabs tested by Deng et al. [27]. Besides, the numerical models also predicted that the use of UHPC in the connection presents a slight increase in the flexural strength capacity in all cases compared to the monolithic concrete model. The variation in the type of joint detail and the geometric shape of the connection had little influence on the flexural capacity. On the other hand, the reinforcement ratio significantly influenced the flexural behavior, which

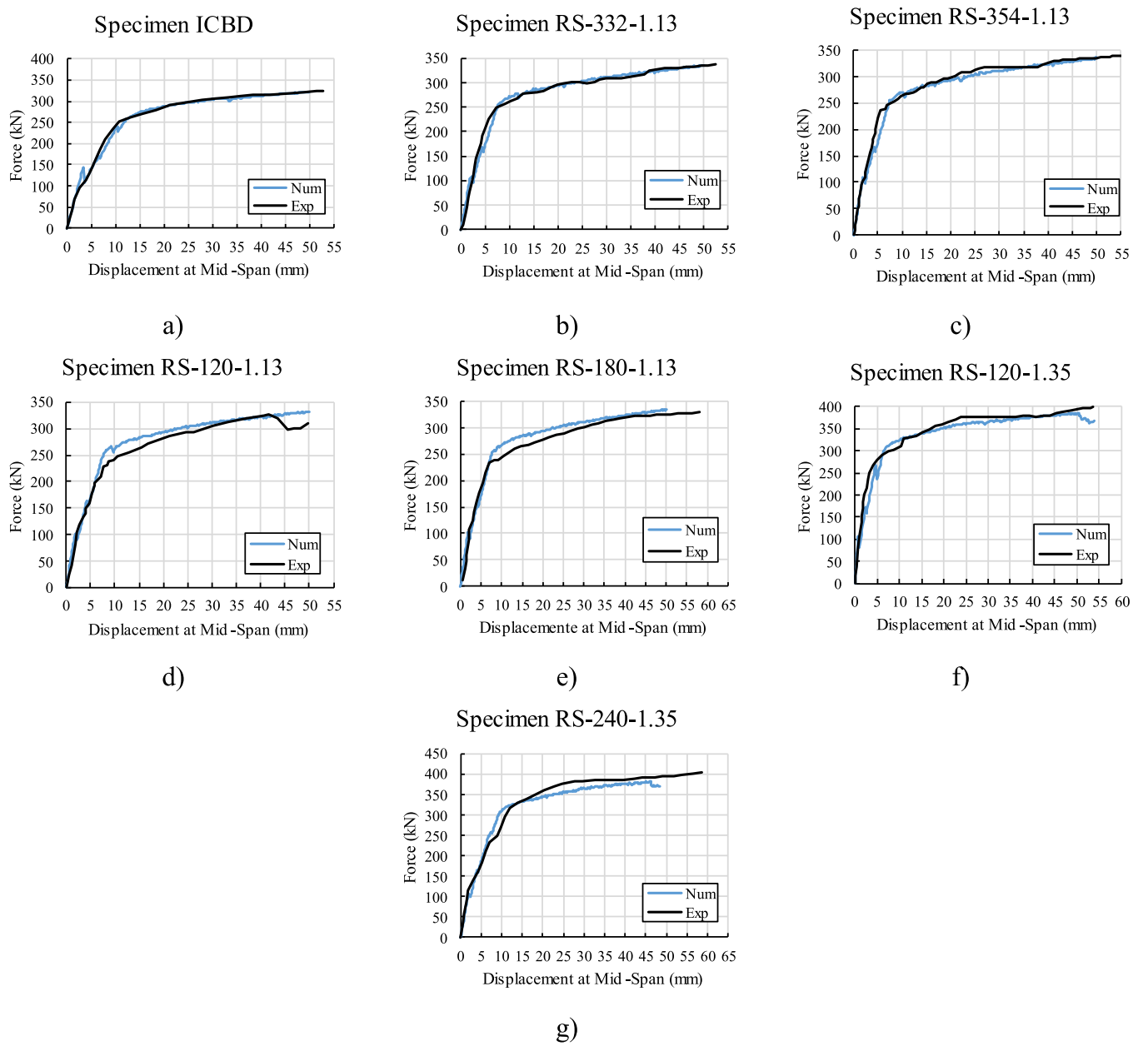

Fig. 11. Comparison of mid-span force-displacement curves from experimental and numerical models.

Table. 8
Comparison between experimental and numerical results regarding cracking load P_{crack}, yielding load P_y and ultimate load P_u.

Model	Specimen	$P_{crack,exp}$ (kN)	$P_{crack,num}$ (kN)	$P_{crack,exp}/P_{crack,num}$	$P_{y,exp}$ (kN)	$P_{y,num}$ (kN)	$P_{y,exp}/P_{y,num}$	$P_{u,exp}$ (kN)	$P_{u,num}$ (kN)	$P_{u,exp}/P_{u,num}$
A	ICBD	87.3	143.2	**0.61**	252.1	258.1	**0.98**	325.3	322.1	**1.01**
B	RA−332–1.13	103.8	109.2	**0.95**	226.0	256.1	**0.88**	338.2	335.2	**1.01**
	RA−354–1.13	98.1	109.2	**0.90**	222.8	254.7	**0.87**	348.2	336.3	**1.04**
C	RS−120–1.13	101.6	101.2	**1.00**	228.5	259.4	**0.88**	327.2	325,3	**1.02**
	RS−180–1.13	97.2	102.0	**0.95**	233.6	252.4	**0.93**	335.4	329.6	**1.02**
D	RS−120–1.35	116.4	107.0	**1.09**	267.2	298.2	**0.89**	399.8	385.4	**1.04**
	RS−240–1.35	115.5	109.2	**1.06**	316.9	302.2	**1.05**	403.4	382.0	**1.06**
AVG				**0,96**			**0,94**			**1,03**
COV				**17,13 %**			**8,29 %**			**1,71 %**

was expected according to the flexural theory.

Fig. 12 shows the comparison between the experimental and predicted cracking pattern by the numerical models for the specimens tested by Deng et al. [27]. The numerical models accurately represented the flexural failure mode of the slabs. The locations of cracking identified in the models closely matched those observed in the flexural tests conducted by Deng et al. [27]. Notably, there was minimal to no visible cracking in the areas of the slabs where UHPC was used, both in the

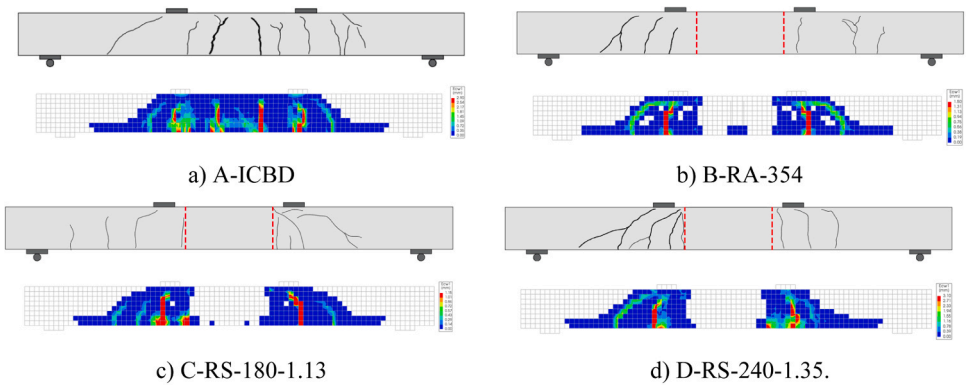

Fig. 12. Comparison between the experimental and predicted cracking pattern by the numerical models for the tests: a) A-ICBD; b) B-RA-354–1.13; c) C-RS-180–1.13 and; d) D-RS-240–1.35.

Table 9
Parameters studied in parametric analyses.

Parameter	Tested values
Overlapping length	$10d_b$; $7{,}5d_b$; $5d_b$; $2{,}5db$; $0db$
Wet joint length	300 mm; 200 mm; 150 mm; 100 mm
Concrete type and compressive strength	52,2 MPa (NSC); 110 MPa (UHPC); 131,3 MPa (UHPC); 150 MPa (UHPC)
Overlapping of rebar connection	Straight; Headed rebar or U-bars

experimental and numerical models.

In the ICBD model, a higher concentration of cracks was observed in the middle of the span. In the models featuring UHPC connections, cracks initiated at the interfaces and then developed at the bottom of the loading point, gradually extending obliquely toward the interface as the load increased, as observed by Deng et al. [27] in the experimental tests.

5. Parametric analyses

It is proposed to investigate the influence of six parameters that can guide the detailing of wet joint connections for bridge decks: (i) overlapping length of rebars, (ii) wet joint length, (iii) concrete compressive strength, (iv) type or shape of rebar connection, (v) reinforcement ratio. In practice, these parameters are some of the most important because they define the amount of UHPC required to fill the connection and the amount of reinforcement needed to ensure adequate structural behavior of the connection. Table 9 presents a summary of the variables studied in this parametric analysis. Fig. 13 illustrates the design parameters of various connections for this analysis.

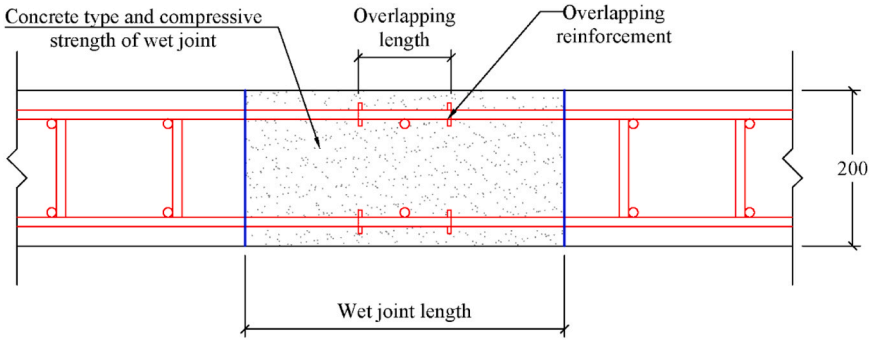

Fig. 13. Description of the design parameters from UHPC wet joints varied in this study.

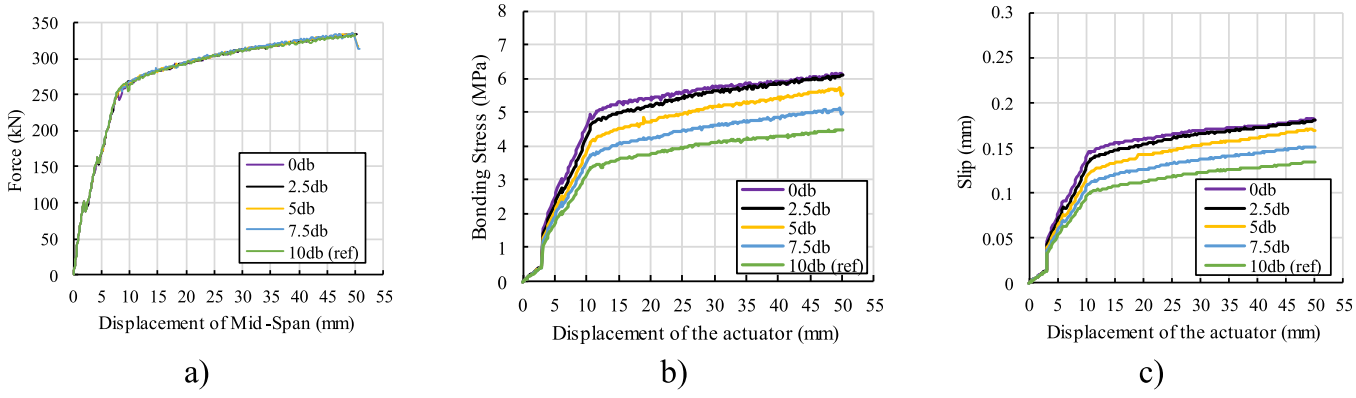

Fig. 14. Influence of the overlapping length of rebars on the a) force–Displacement curve; b) Bonding stress–Displacement of the actuator and c) slip–displacement of the actuator.

Table 10
Relationship between the maximum bond stress measured from the numerical model and the ultimate bond stress inputted in the bond-slip model.

Model	Maximum bond stress from numerical model τ (MPa)	Ultimate bond stress τ_u (MPa)	τ/τ_u
$10d_b$ (ref)	4.49	17.35	0.259
$7.5d_b$	5.10	17.38	0.294
$5d_b$	5.71	17.43	0.328
$2.5d_b$	6.11	17.47	0.350
$0d_b$	6.14	17.52	0.351

For the parametric study, the calibrated numerical model RS-120–1.13 was selected as the reference for the material and geometric properties. This model has the following key characteristics: (i) an overlapping length of 120 mm ($10d_b$), (ii) a flexural reinforcement ratio of 1.13 %, (iii) a rectangular connection shape, and (iv) straight reinforcement at the ends.

5.1. *Influence of overlapping length of rebars*

Fig. 14a shows the effect of the varied overlapping length on the force−displacement in the middle of the span graphs. The results indicate that variations in the overlapping length of the reinforcement, including cases where the length is zero, did not affect the behavior of the structure when UHPC was used. Consequently, none of the models exhibited anchorage failure. It should be mentioned that Graybeal (2014) found good performance by straight rebars with lengths equal to or less than $8d_b$ for longitudinal joints made of UHPC. The general suggestion of AASHTO [30] loop spliced is the basic anchorage length.

To further examine the bonding behavior between longitudinal reinforcements in the models, the maximum bond stress and the slip at the reinforcement end were analyzed as a function of the displacement applied by the hydraulic actuator (Fig. 14b,c). Table 10 shows the maximum bond stress for each model and their respective ultimate bond stresses at the wet joint. The analytical model proposed by Pan et al. [25] was used to evaluate the ultimate bond stress, since the ultimate stress in this model varies with the anchorage length of the steel bar. Fig. 14b shows that reducing the splice length results in an increase in the bond stress of reinforcement. However, the maximum bond stress obtained is significantly lower than the ultimate bond stress, making it very unlikely that the reinforcement anchorage failure will occur. The maximum bond stress reached is 35.1 % of the ultimate bond stress when reducing the splice to zero. Fig. 14c shows that the relative slip is small and doesn't depend significantly on the length of the lap splice. When using UHPC, the overlap length of reinforcements is reduced due to the high bond strength.

The maximum bond stress for each model, along with their respective limit bond stresses at the wet joint, is summarized in Table 10. These values are calculated based on using the model by Pan et al. [25], which shows that the ultimate stress varies depending on the length of the steel bar at the connection point.

The small influence of the length of the reinforcement lap splice is justified by the long length of the wet joint (412 mm) and the better tensile strength of UHPC. Thus, the connection, according to the numerical models, is strong enough to transmit the forces between the precast slabs with little or no overlap length. In this context, it is found that, considering high-strength concrete, only the variation of the length of the reinforcement lap splice has little influence on the bending behavior of the structure due to the mechanical properties and geometry of the connection. Therefore, it is essential to investigate the variation in the overlap length for different wet joint lengths.

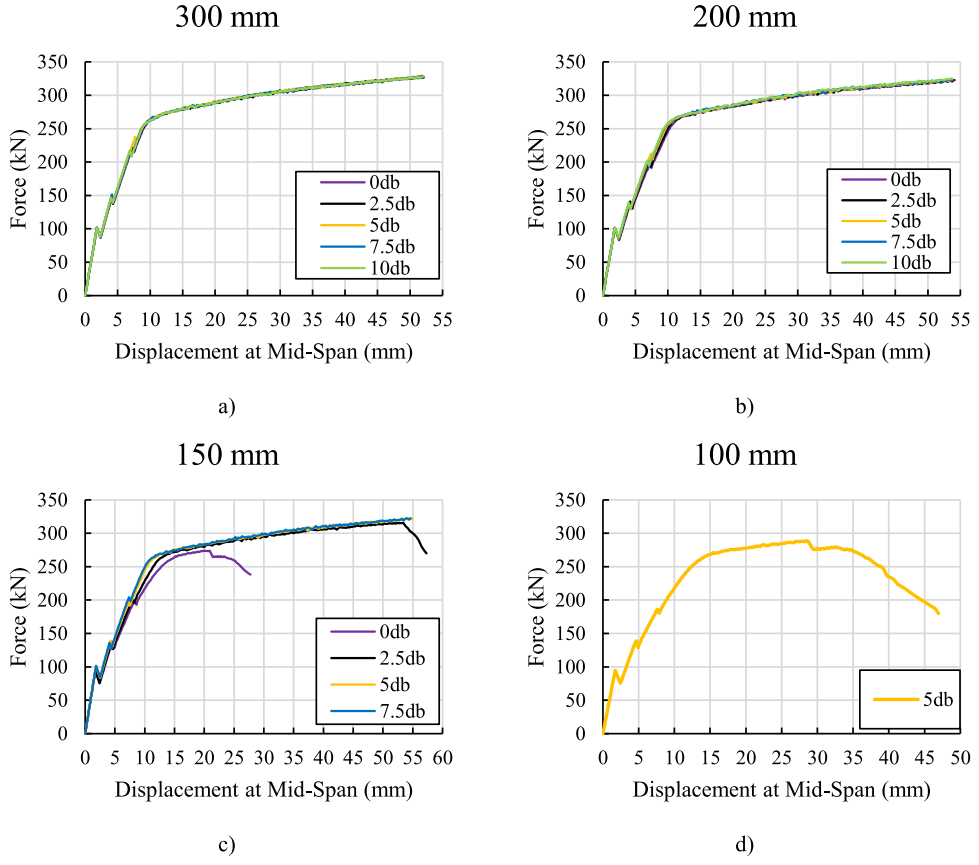

Fig. 15. Load−displacement curve of the slabs considering wet joint lengths of a) 300 mm; b) 200 mm; 150 mm and d) 100 mm.

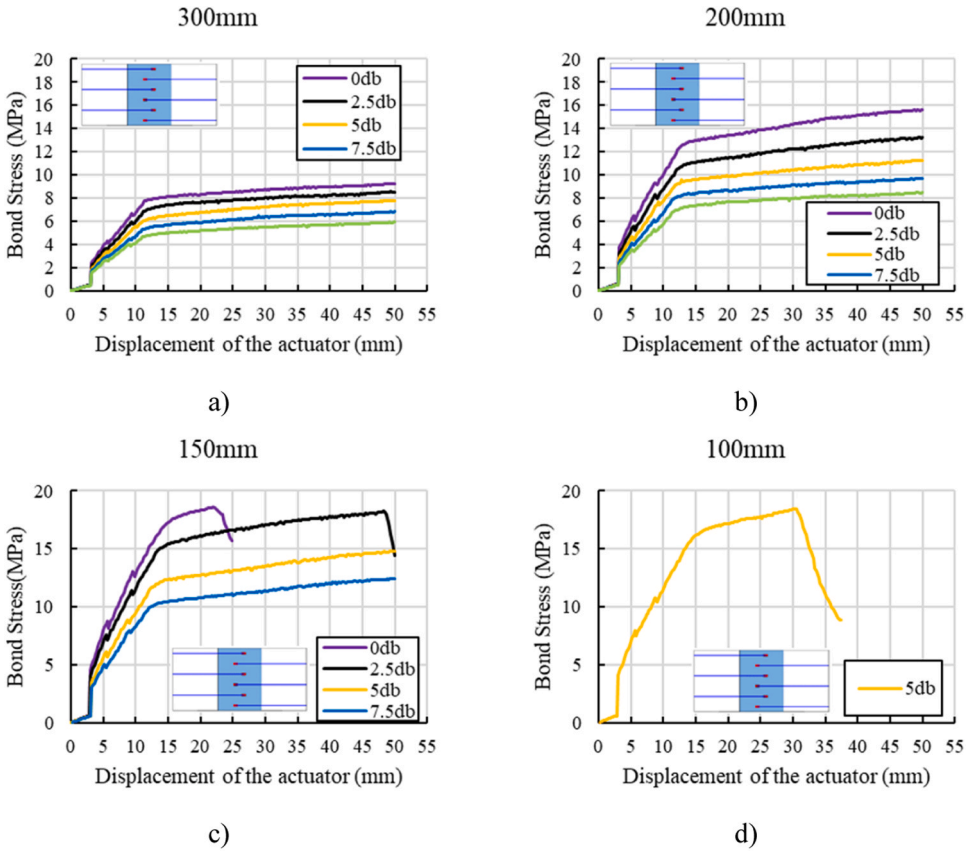

Fig. 16. Bonding stress at the end of the reinforcement in the connection with wet joint lengths of: a) 300 mm; b) 200 mm; c) 150 mm; and d)100 mm.

5.2. *Influence of the wet joint length*

As seen previously, the 412 mm connection length investigated in the experimental studies by Deng et al. [27] becomes too large, so the variation in the overlapping length has little influence on the structure's behavior. In this way, this item investigates the influence of the length of the wet joint combined with overlapping length variations. Therefore, wet joint lengths with UHPC of 300 mm, 200 mm, 150 mm, and 100 mm were selected for this analysis. For each length of wet joint, the splice length of the bars was varied to identify possible failures due to reinforcement anchorage. The results of the variation in lap splice length as a function of the length of wet joint are presented in Fig. 15.

Fig. 15 shows that anchorage failure begins to occur in models with a wet joint length of 150 mm. If the overlapping length is reduced to $2.5d_b$, a sharp drop in resistance can be observed with displacement in the middle of the span of approximately 53 mm. By reducing the lap splice length to zero, failure occurs much earlier. For a wet joint length of 100 mm, it is already possible to observe the occurrence of failure for the largest length of $5d_b$.

Fig. 16 shows the bond stress at the end of the longitudinal bars as a function of the displacement of the hydraulic actuator to verify whether the failures occurred due to anchoring. The relative slip between the reinforcement and the UHPC is observed in Fig. 17. Table 11 presents the results of the maximum bond stress of each model and their respective ultimate bond stress of the reinforcement in the wet joint connection with UHPC.

As observed in Fig. 16 and Table 11, the bond stress at the end of the reinforcement reaches the ultimate bond stress in the models with a wet joint length of 150 mm using overlapping length of 2.5 d_b and for a wet joint length of 100 mm using overlapping length of 5 d_b. The anchorage failure can also be observed in Fig. 17 by the exponential increase in slip when the limit stress is reached. Therefore, anchorage failure is avoided by using a wet joint length of at least 200 mm and a lap splice length of at least $7.5d_b$.

According to Graybeal [31], for UHPC with a 2 % fiber content, a minimum splice length of $8d_b$ is recommended for steel bars with a yield strength (f_y) below 517 MPa, diameter's bar greater than 8 mm and cover thickness (c) is not less than $3d_b$. For a cover thickness of $2d_b \leq c \leq 3d_b$, as in the case of the tested numerical models, a length of $10d_b$ is suggested. Therefore, the results of the parametric analysis align with Graybeal [31] recommendations.

It is noteworthy that when the joint length exceeds 200 mm, the UHPC connections are sufficient to transfer the internal forces between the different precast slabs, even without any reinforcement overlap, as the high tensile strength of UHPC significantly enhances the flexural strength of the section. At this point, the anchorage failure can be suppressed just by providing sufficient reinforcement length embedded in the wet joint connection.

5.3. *Influence of the concrete used in the wet joint*

Using the RS-120–1.13 reference model, the influence of the material used for the wet joint connection was investigated. First, the wet joint filled by UHPC was compared with the wet joint filled by normal strength concrete ($f_c = 52.2$ MPa), the same considered for precast slabs, adopting the same overlapping length of 120 mm (10 d_B). The results of the force−displacement curve is presented in Fig. 18a.

Fig. 18a shows that when using normal concrete in the connection, the structure fails prematurely, while the model with UHPC demonstrates a higher bearing capacity. An analysis of the reinforcement bond stress in the wet joint revealed that the model with $f_c = 52{,}2$ MPa quickly reached the ultimate bond stress, which, based on the equations presented in Table 3, is $\tau_u = 10.10$ MPa (Fig. 18b). When this occurs, the reinforcement anchorage will fail (Fig. 18c). In the model with the

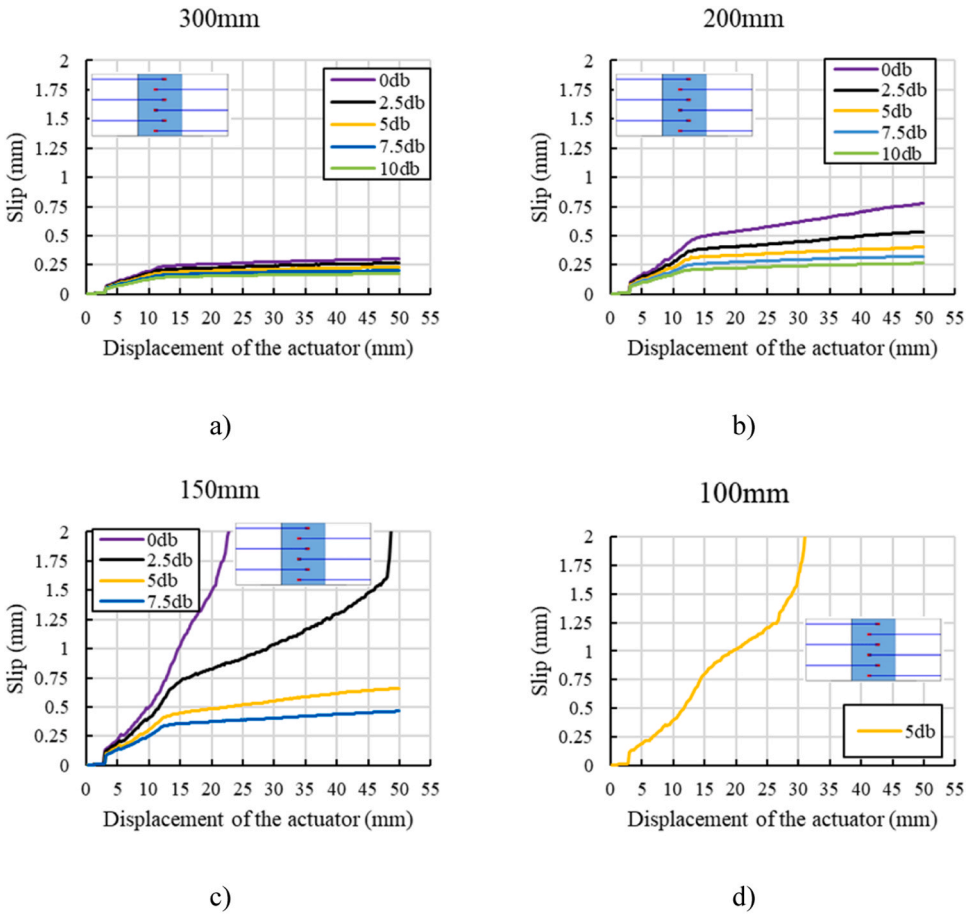

Fig. 17. Relative slip of reinforcement in the connection with wet joint lengths of a) 300 mm; b)200 mm; c) 150 mm; d) 100 mm.

connection with UHPC, the maximum bond stress reached at the end of the bar in the numerical models is 4.47 MPa, lower than the ultimate bond stress of $\tau_u = 17.35$ MPa.

Fig. 19 and Fig. 20 show the bond stress distribution of the models with NSC and UHPC in the load steps of the elastic stage at the point after the first crack and the maximum load, respectively. The curves show little difference in bond stresses between the connections with normal concrete and UHPC until the first crack. It can be highlighted that until the elastic stage, the maximum bond stress values are predominant at the ends of the bars, and after the first crack, the maximum stresses occur at the interface of the connection with the precast slabs.

At the maximum load, the bond stresses in the reinforcement of the normal concrete connection model reach the ultimate bond stress for conventional concrete, with stress concentration in the length of the lap splice. However, for the UHPC connection, the shape of the stress diagram remains unchanged after the first crack. This is because the bond stress is too low to reach the ultimate bond stress.

Fig. 21 and Fig. 22 show the concrete strain and principal compressive stress directions at the maximum load in the plane of the bottom reinforcement in the wet joint. Fig. 21a shows that, in wet joint with normal concrete, a tensile strain is located between lap spliced reinforcements. However, in the wet joint with UHPC, as shown in Fig. 21b, the predominant tensile strain is in the interface between UHPC and precast panels, with a considerably smaller magnitude. Fig. 22a shows that compression struts are formed in the plane of the bottom reinforcements in the wet joint with normal concrete. However, in wet joint with UHPC, as illustrated in Fig. 22b, it is observed that the predominant tensile stresses are parallel to the bottom reinforcement. Therefore, it can be concluded that the formation of struts does not occur for the model with a wet joint filled with UHPC.

The absence of bar slippage in the concrete, due to the high tensile strength of UHPC, is one explanation for this phenomenon. In the wet joint with a UHPC, pure bending occurs at the overlap, whereas in conventional concrete, there is a disturbance caused by the anchorage, which distributes stresses as struts to transfer the load. In UHPC, the principal stresses resemble those of a beam with continuous reinforcement. As a result, force transfer that would normally arise from reinforcement slippage does not occur. This causes uniform tension of the concrete by the anchorage, ensuring the complete transfer of the tensile resultant at the joint without the formation of struts.

5.4. *Influence of the compressive strength of UHPC*

An analysis was performed by varying the compressive strength of the concrete (f_c) used in connection with values of 110 MPa, 131.3 MPa (reference), and 150 MPa. The modulus of elasticity of UHPC in this analysis was estimated from the Equation of Guo et al. [32].

$$E_c = 3837\sqrt{f_c} \tag{17}$$

The maximum bond stress between the reinforcement and the UHPC is also defined from the model by Pan et al. [25]. Table 12 presents the values used in the numerical analyses performed for each concrete strength. The results due to the variation in the compressive strength of the connection are presented in terms of the load−displacement curve at mid-span. In Fig. 23a shows that the variation in the UHPC strength had little influence on the flexural behavior of the models. As previously observed, this result may be related to the large wet joint length with UHPC. When reducing the concrete's compressive strength to 110 MPa, the bond behavior remains similar to the reference model. Fig. 23b shows that in the model with UHPC of 110 MPa, failure occurred more

Table 11
Relationship between the maximum bond stress measured in the numerical model τ and the calculated ultimate bond stress τ_u.

Wet joint length (mm)	Overlapping length	Maximum bond stress from numerical model (MPa)	Ultimate bond stress τ_u (MPa)	τ/τ_u	Anchorage failure
300	$10d_b$	5,93	17,51	0,34	No
	$7{,}5d_b$	6,85	17,56	0,39	No
	$5d_b$	7,78	17,63	0,44	No
	$2{,}5d_b$	8,57	17,71	0,48	No
	$0d_b$	9,25	17,80	0,52	No
200	$10d_b$	8,49	17,74	0,48	No
	$7{,}5d_b$	9,71	17,83	0,54	No
	$5d_b$	11,27	17,96	0,63	No
	$2{,}5d_b$	13,25	18,11	0,73	No
	$0d_b$	15,63	18,31	0,85	No
150	$7{,}5d_b$	12,42	18,05	0,69	No
	$5d_b$	14,81	18,23	0,81	No
	$2{,}5d_b$	18,27	18,27	1,00	Yes
	$0d_b$	18,60	18,60	1,00	Yes
100	$5d_b$	18,47	18,47	1,00	Yes

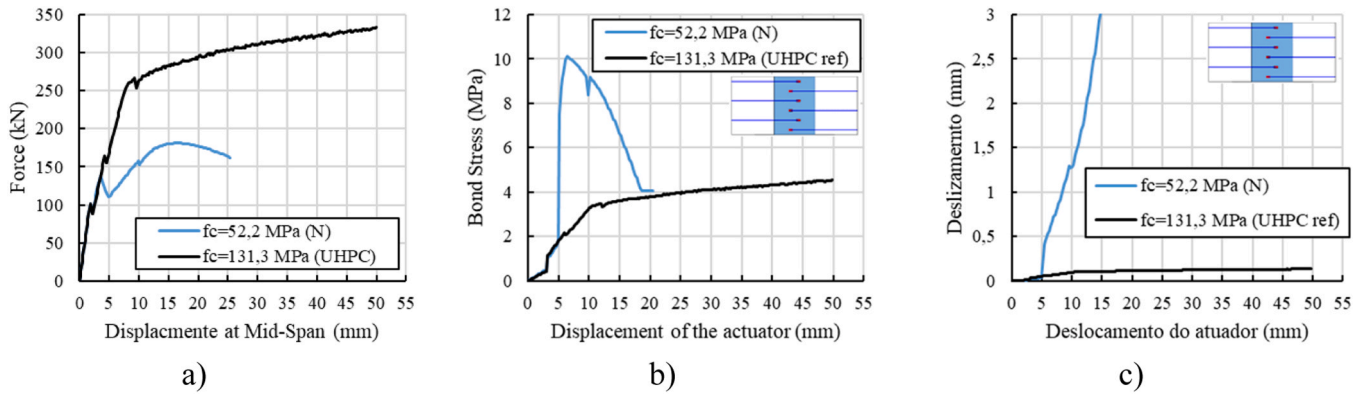

Fig. 18. Influence of the concrete used for filling the wet joint a) Force–displacement ate mid-sepn curve; b) bond stress at the bar end versus actuator displacement; c) bar end slip versus actuator displacement.

quickly than in the reference model of 131.3 MPa, with the failure mode also being due to insufficient anchorage length of the bars.

Fig. 24 illustrates the influence of the UHPC strength on different wet joint lengths. In this analysis, the length of the lap splice remained constant with a $2.5d_b$. The results indicate that resistance of the connection was influenced by both the wet joint length and the UHPC strength. Increasing concrete's compressive strength, which increases the concrete's tensile strength and ultimate bonding stress, normally improves the anchoring properties of the reinforcement. Therefore, when the compressive strength was increased from 110 MPa to 150 MPa, the resistance of the model with a wet joint length of 100 mm was increased by 17,1 %. However, at wet joint lengths greater than 150 mm, there was less influence on the strength of the UHPC.

5.5. *Influence of the type of rebar connection*

The type of reinforcement detailing in the connection was investigated by testing the following types of details: straight bars, headed bars, and U-shaped bars (annular reinforcement). Since the straight bar model has already shown good anchorage results for the reference model, an analysis was performed of the variation in reinforcement detail in the connection of the model with a wet joint length of 150 mm and an overlapping length of $2.5d_b$. Fig. 25 shows the details of the type of reinforcement used in the parametric analysis.

In the model with headed bars (Fig. 25b), the mechanical anchorage was modeled with solid elements connected to the longitudinal bars to allow the representation of possible concrete crushing at the ends and the anchor effect. Interface properties with high rigidity between the reinforcement head and the concrete were also considered. In the case of the U-shaped bars, it was not possible to represent the full curve because

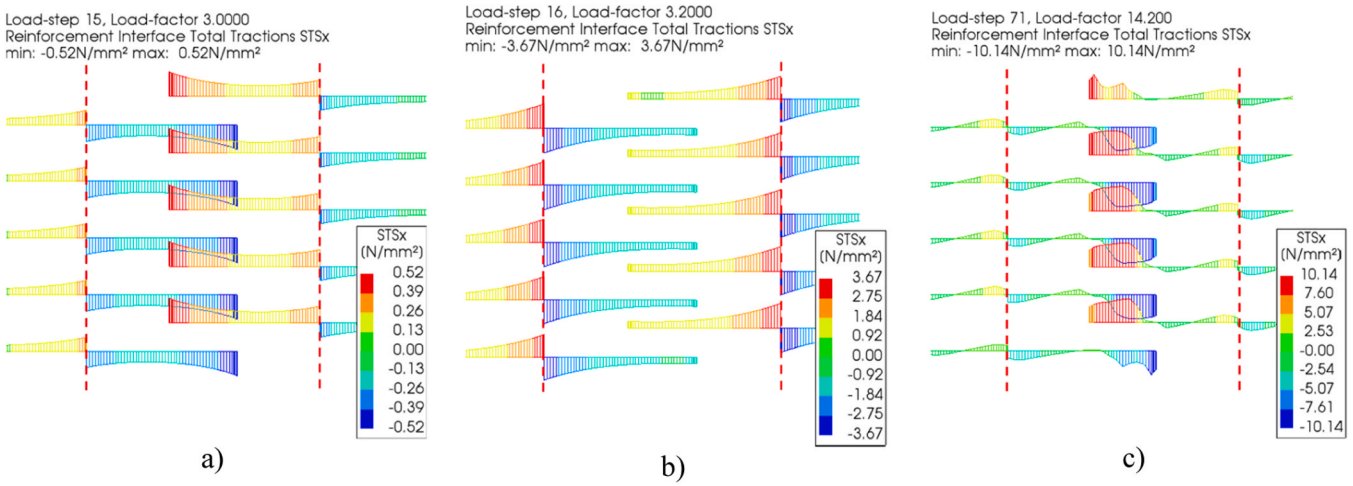

Fig. 19. Reinforcement bond stress distribution for the wet joint with NSC. a) Before the first crack (elastic stage); b) After the first crack; c) Point of maximum load.

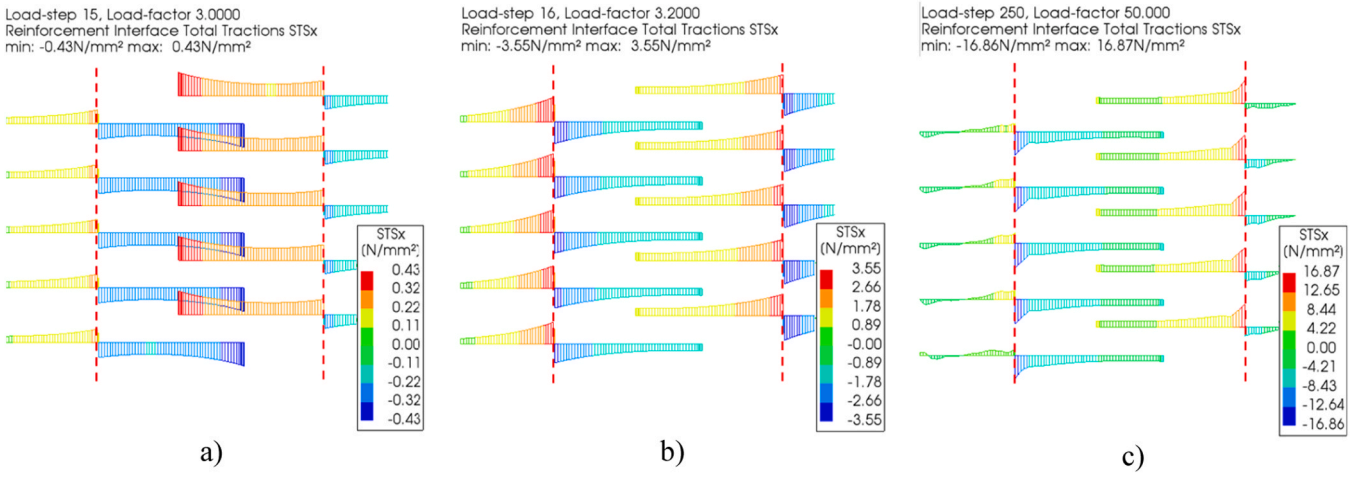

Fig. 20. Reinforcement bond stress distribution for the wet joint with UHPC: a) Before the first crack (elastic stage); b) After the first crack; c) Point of maximum load.

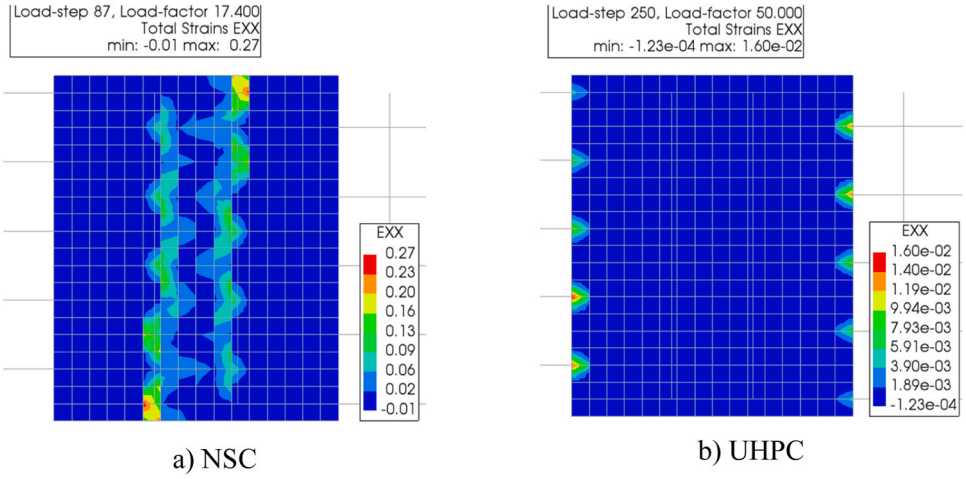

Fig. 21. Concrete strain in the wet joint at the maximum load using a) NSC and b) UHPC as filling material.

of the limited overlapping length (30 mm). In this case, the minimum bending diameter of $3d_b$ (36 mm) was considered in the reinforcement curve. At this point, it should be noted that the minimum bend diameter recommended by the normative codes was not respected. Nonetheless, these bend diameters were derived for use with normal-strength concrete and shall be revised for UHPC in future investigations.

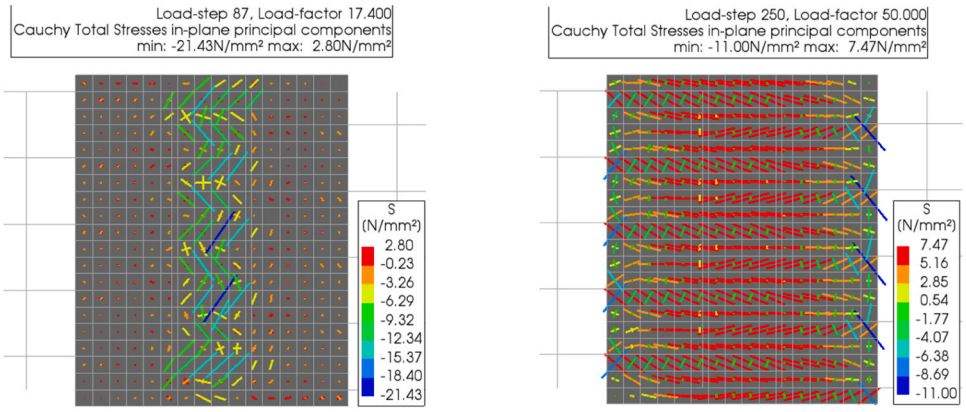

Fig. 22. Plan view direction of the principal compressive stresses in the wet joint connection at maximum load for: a) NSC and b) UHPC as filling material.

Table 12
Main concrete properties considered in the analysis of UHPC strength.

Compressive strength f_c (MPa)	Tensile strength f_t (MPa)	Modulus of elasticity (MPa)	Ultimate bond stress τ_u (MPa)
110	6,89	40,240	15,88
131,3*	7,75	41,400*	17,35
150	8,48	46,990	18,34

* Experimental value

Fig. 26 shows the influence of various reinforcement details in the load–displacement curve of the slabs. In practice, Fig. 26 shows that changing the type of reinforcement detail has minimal impact on the resistance and flexural behavior of the models. This is attributed to the sufficient length of the wet joint used in this analysis, which increases the contact area between the reinforcement and the concrete. However, the brittle failure observed by the straight bars slippage was no longer observed in the models with the headed bars and the U-shaped bars.

Fig. 27, Fig. 28, and Fig. 29 illustrate the bonding stress distribution in the reinforcement along the loading history, which is, in the elastic behavior, at the point of first crack and the maximum load. These figures

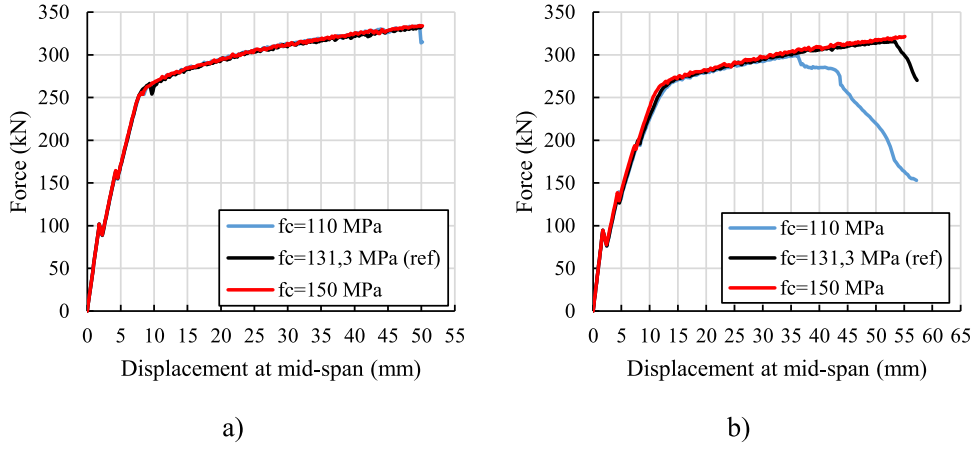

Fig. 23. a) Load–displacement curve for different compressive strength of the UHPC, considering a wet joint length of 412 mm and an overlapping length of 120 mm (10 d_b); b) considering a connection length of 150 mm and an overlapping length of 30 mm (2.5 dB).

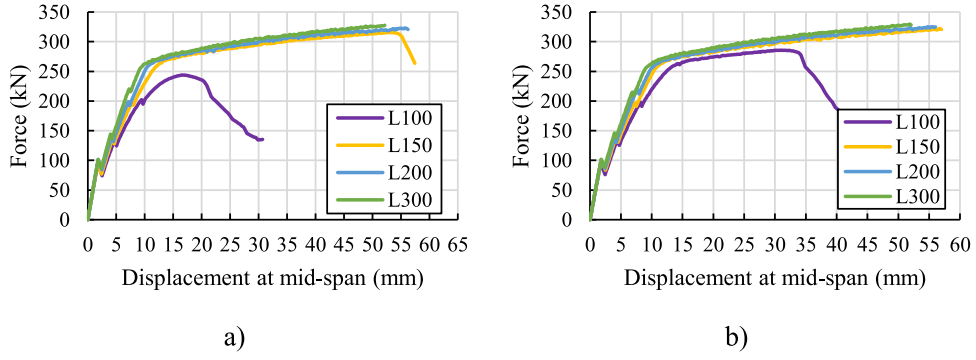

Fig. 24. Load–displacement curve for different compressive strength of the UHPC: a) 110 MPa and an overlapping length of 30 mm (2.5 d_b); b) 150 MPa and an overlapping length of 30 mm (2.5 d_b).

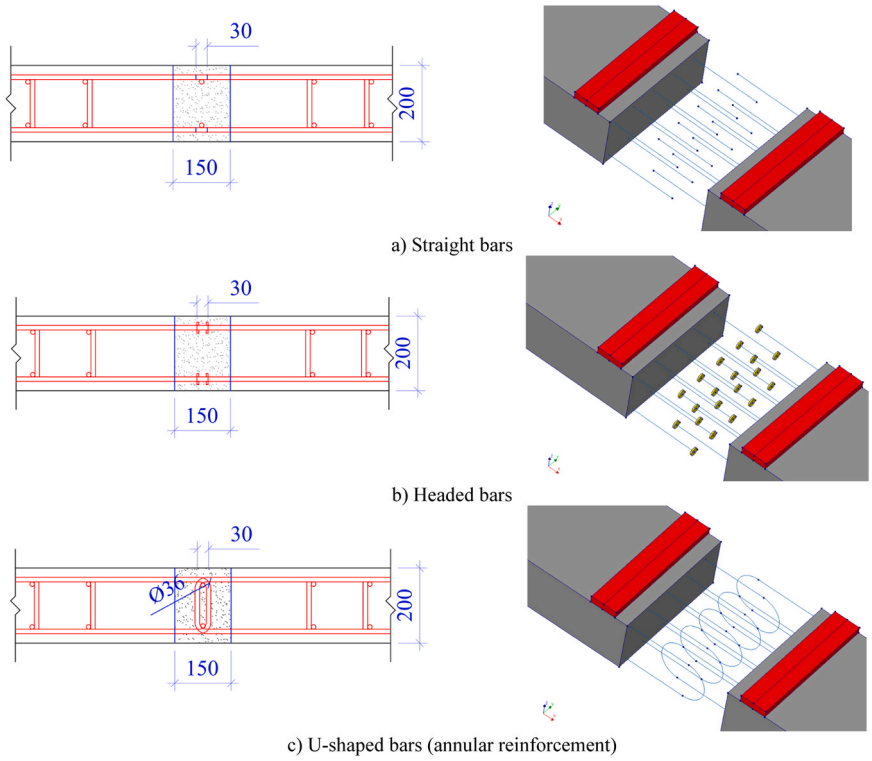

Fig. 25. Type of rebar connection considered in the numerical models.

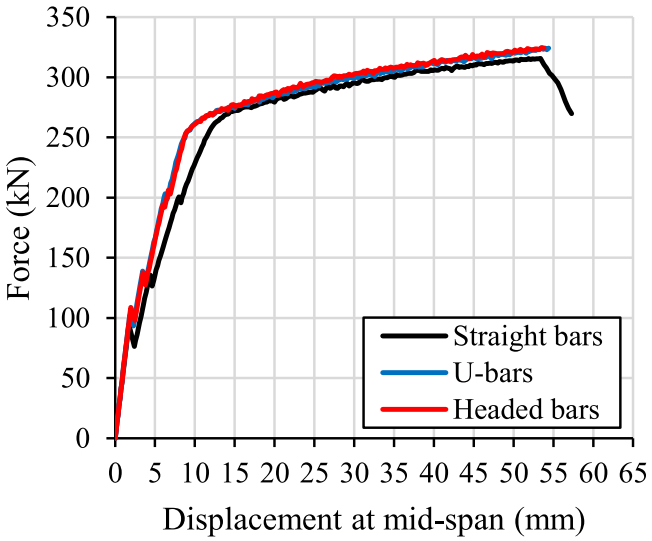

Fig. 26. Influence of the type of rebar connection on the load−displacement curve of the slabs with a wet joint length of 150 mm.

clearly indicate that using alternative reinforcement details in the wet joint connection, such as headed bars or U-shaped bars, effectively helps prevent anchorage failure. In the model with headed bar, the bond stress at the bar ends is almost zero, while in the model with U-shape bar, it is almost zero at the curvature. In both cases, the highest probability of anchorage failure occurs near the interface of the wet joint with precast concrete. Therefore, the results demonstrate that incorporating different reinforcement details into the connection can be an effective strategy for reducing the length of the connection.

6. Discussions

This paper presented a detailed analysis on the behavior of wet joints filled with UHPC and overlapping of longitudinal reinforcement. Compared to previous publications on this field, we highlighted the importance of a detailed modelling of the bond-slip properties of the reinforcement to the proper representation of possible anchorage failures on such joints. Based on that, the proposed modelling strategy may be applied to simulate other types of connections from bridge deck slabs using UHPC. Besides that, we investigated in the parametric analyses the influence of the overlapping length of longitudinal rebars, wet joint length, concrete type, compressive strength of UHPC and type of rebar connection. Nevertheless, other important parameters still need to be investigated in future publications.

For example, the influence of the transverse reinforcement ratio on preventing splitting failure was not explored in this study. In this context, Huang et al. [33] already shown that the absence of proper transverse reinforcement amount would significantly reduce the ultimate capacity of the U-bar joints. Besides, these authors also showed that increasing the transverse reinforcement amount upon a determined value was not helpful in promoting the ultimate capacity of specimens. Therefore, further studies on this topic should be performed to determine specifical recommendations for each type of reinforcement detailing. Besides, the influence of fatigue loading on the behavior and capacity of such joints is also another aspect that should be addressed in future investigations experimentally and numerically.

Regarding the investigation related to the type of rebar detailing, the presented results demonstrate that the U-shaped bars are effective, even with narrower joint widths, made of UHPC. The remaining challenges are ensuring adequate durability (UHPC compaction and rebar cover) and constructability (the arrangement and installation of looped bars must be practical and efficient for field construction), while maintaining accelerated construction features. Nevertheless, crack control and force transfer mechanisms have been proven effective in combining loop connections with UHPC.

Between the main current challenges in this kind of bridge is to

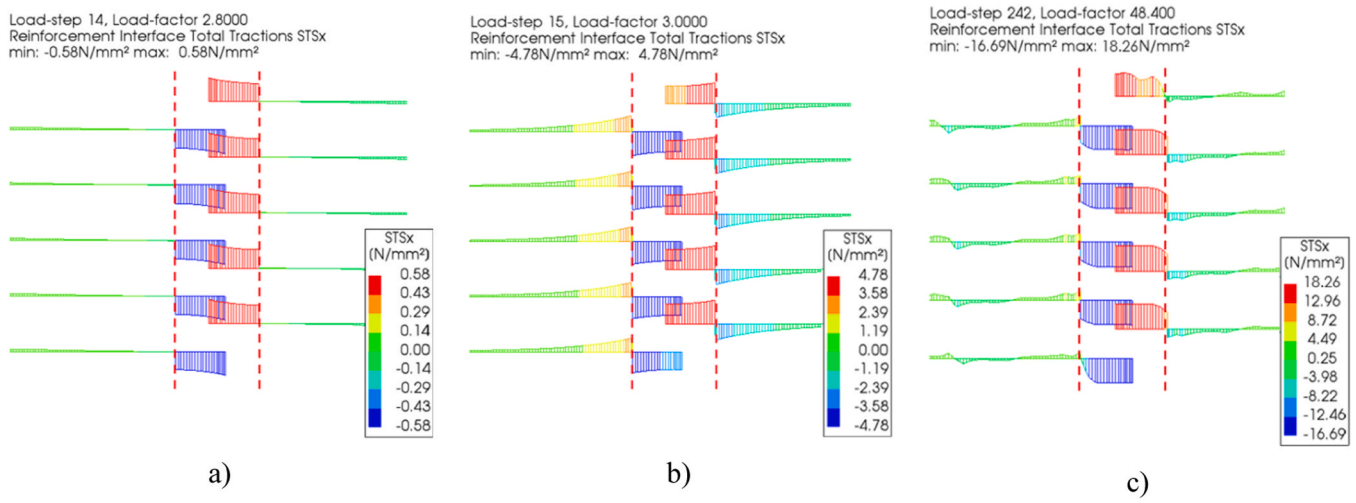

Fig. 27. Reinforcement bonding stress distribution in the model with a straight bar. a) Before the first crack; b) After the first crack; c) Point of maximum load.

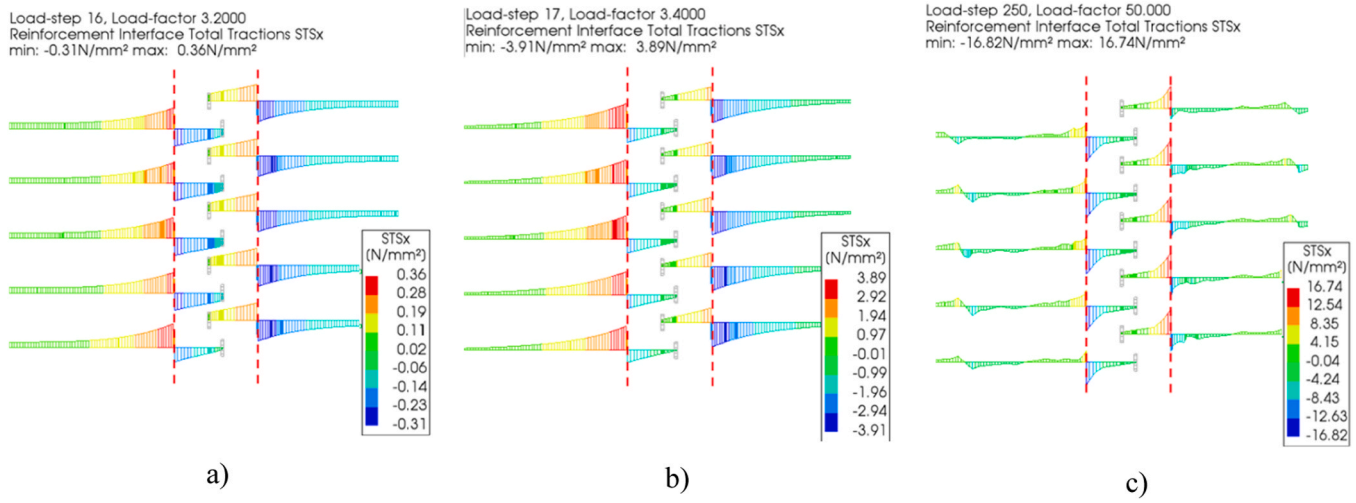

Fig. 28. Reinforcement bonding stress distribution in the model with a headed bars. a) Before the first crack; b) After the first crack; c) Point of maximum load.

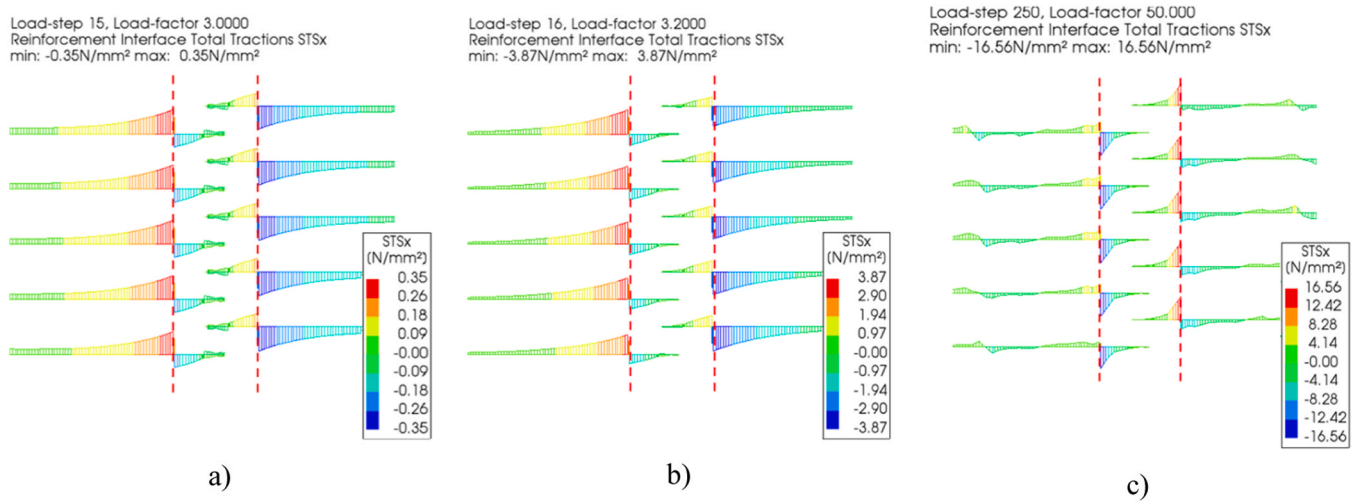

Fig. 29. Reinforcement bonding stress distribution in the model with U-shaped bars. a) Before the first crack; b) After the first crack; c) Point of maximum load.

ensure adequate internal forces transfer between the precast slabs using narrow connections to decrease the amount of UHPC cast in place. In this context, we observed that even narrower connections than those tested in the literature could ensure proper anchorage resistance. Besides that, the detailing of the longitudinal rebars is another point of frequent worry, as the width of the joints is narrow, and U-bars or mechanical anchorage would be recommended. Nevertheless, we observed that the behavior of straight bars will be almost that of mechanically anchored bars and U-shaped bars if an adequate development length is provided for the straight bars.

Another practical aspect addressed in this paper was the comparison between different specimens using normal strength and UHPC as filling material (Fig. 18). Besides a lower cracking strength, the use of normal-strength concrete instead of UHPC would require a much larger connection width to achieve the same ultimate capacity and avoid anchorage failure. Therefore, the use of UHPC stands out not only in terms of service behavior but also in decreasing the amount of cast-in-place concrete, which promotes accelerated bridge construction. Besides that, it shall be noted that using UHPC instead of normal-strength concrete also reduces the concern with concrete crushing in the joint.

7. Conclusions

This study investigates various ultra-high-performance concrete (UHPC) connection design configurations for precast slabs with wet joints through Finite Element Method (FEM) analysis. Numerical models accurately replicated experimental results, predicting failure mechanisms and load-bearing capacities with an experimental-to-numerical strength ratio averaging 1.03 and a coefficient of variation of 1.71 %. Furthermore, as observed experimentally, all numerical models accurately represented the failure mechanism, which was governed by the yielding of the longitudinal reinforcement in the precast concrete region.

Additionally, a parametric analysis explored the impact of varying UHPC connection configurations. The main recommendations are listed below:

- For models with UHPC and wet joint length of 412 mm, reducing lap splice length from $10d_b$ to $0d_b$ had minimal impact on flexural behavior of precast slabs due to UHPC's high tensile strength. In these cases, the UHPC would be sufficient to transfer internal forces between the different precast panels, even without any overlapping reinforcement. Therefore, for such cases, it would be necessary to ensure that only a certain length of reinforcement is embedded within the UHPC connection to avoid anchorage failure.
- Bond failure occurred when wet joint lengths were below 200 mm and overlapping lengths were less than $7.5d_b$, aligning with Graybeal's [31] recommendations, which indicated the possibilities of slipping of steel bars when the embedment length is less than 8_{db}.
- Slabs with NSC (compressive strength of 52.2 MPa) experienced a brittle anchorage failure, while UHPC slabs (131.3 MPa) showed a reduced risk of strut compression failure. Compressive strength variations of UHPC (110 MPa, 131.3 MPa, and 150 MPa) did not affect failure mechanisms unless wet joint lengths were reduced to 150 mm and overlapping lengths to 30 mm. In these cases, slabs with 150 MPa UHPC exhibited flexural failure, while lower compressive strengths (131.3 MPa and 110 MPa) led to anchorage failure.
- Reinforcement type influenced failure mechanisms in models with wet joint lengths of 150 mm and overlapping lengths of 30 mm. Straight bars caused anchorage failure, while headed bars and U-shaped bars improved anchorage resistance, enabling potential reductions in wet joint length.

The findings emphasize UHPC's tensile strength, lap splice length, and reinforcement type as critical factors in optimizing connection design and preventing anchorage failure in wet joints for precast slabs

CRediT authorship contribution statement

Pablo Augusto Krahl: Writing – review & editing, Visualization, Methodology. **Mounir Khalil El Debs:** Writing – review & editing, Supervision, Methodology, Funding acquisition, Conceptualization. **Daniel de Lima Araújo:** Writing – review & editing, Visualization, Software, Resources, Methodology. **Rafael Sanabria Díaz:** Software, Methodology. **do Rosario da Silva Marcos Antonio:** Writing – review & editing, Writing – original draft, Visualization, Validation, Software, Methodology, Investigation, Formal analysis, Data curation. **Dantas de Sousa Alex Micael:** Writing – review & editing, Writing – original draft, Visualization, Supervision, Project administration, Methodology, Investigation, Conceptualization.

Declaration of Competing Interest

The authors declare that they have no known competing financial interests or personal relationships that could have appeared to influence the work reported in this paper.

Acknowledgments

The authors acknowledge the financial support provided by the São Paulo Research Foundation (FAPESP), grant number 2024/13561–5; and by the Brazilian National Council for Scientific and Technological Development (CNPq), grant number 405500/2022–0.

References

[1] Culmo M.P. Connection details for prefabricated bridge elements and systems. 2009.
[2] Wang X, Liu Y, Chen A, Ruan X. Flexural capacity assessment of precast deck joints based on deep forest. Structures 2022;41:270–86. https://doi.org/10.1016/j.istruc.2022.05.009.
[3] Jia J, Ren Z, Bai Y, Li J, Li B, Sun Y, et al. Tensile behavior of UHPC wet joints for precast bridge deck panels. Eng Struct 2023;282:115826. https://doi.org/10.1016/J.ENGSTRUCT.2023.115826.
[4] Tan X, Mahjoubi S, Zhang Q, Dong D, Bao Y. A framework for improving bridge resilience and sustainability through optimizing high-performance fiber-reinforced cementitious composites. J Infrastruct Preserv Resil 2022;3:1–18. https://doi.org/10.1186/S43065-022-00067-0/TABLES/1.
[5] Du J, Tan X, Wang Y, Bao Y, Meng W. Reducing the cracking potential of ultra-high-performance concrete (UHPC) with the prewet expansive agent. Constr Build Mater 2024;431:136597. https://doi.org/10.1016/J.CONBUILDMAT.2024.136597.
[6] Tan X, Du J, Zhang Q, Meng W, Bao Y. Monitoring restrained shrinkage and cracks of ultra-high-performance concrete (UHPC) using distributed fiber optic sensors. Constr Build Mater 2024;422:135789. https://doi.org/10.1016/J.CONBUILDMAT.2024.135789.
[7] Tian J, Wu X, Tan X, Zuo Y, Zheng Y, Yuan J, et al. Feasibility study of smart functional strain-hardening cementitious composites: self-sensing model and experimental performance. Constr Build Mater 2024;436:136850. https://doi.org/10.1016/J.CONBUILDMAT.2024.136850.
[8] Haber ZB, Graybeal BA. Lap-spliced rebar connections with UHPC closures. J Bridge Eng 2018;23:04018028. https://doi.org/10.1061/(ASCE)BE.1943-5592.0001239.
[9] Alkaysi M, El-Tawil S. Factors affecting bond development between ultra high performance concrete (UHPC) and steel bar reinforcement. Constr Build Mater 2017;144:412–22. https://doi.org/10.1016/J.CONBUILDMAT.2017.03.091.
[10] Vella JP, Vollum RL, Jackson A. Flexural behaviour of headed bar connections between precast concrete panels. Constr Build Mater 2017;154:236–50. https://doi.org/10.1016/J.CONBUILDMAT.2017.07.146.
[11] Ma ZJ, Lewis S, Cao Q, He Z, Burdette EG, French CEW. Transverse joint details with tight bend diameter U-bars for accelerated bridge construction. J Struct Eng 2012;138:697–707. https://doi.org/10.1061/(asce)st.1943-541x.0000518.
[12] Hussein HH, Walsh KK, Sargand SM, Steinberg EP. Interfacial properties of ultrahigh-performance concrete and high-strength concrete bridge connections. J Mater Civ Eng 2016;28:04015208. https://doi.org/10.1061/(ASCE)MT.1943-5533.0001456.
[13] Di J, Han B, Qin F. Investigation of U-bar joints between precast bridge decks loaded in combined bending and shear. Structures 2020;27:37–45. https://doi.org/10.1016/j.istruc.2020.05.041.
[14] Hu J, Gu Y, Yan J, Sun Y, Huang X. Experimental study on flexural resistance of UHPC wet joint precast reinforced concrete bridge deck slabs with variable cross-section. Appl Sci 2024;14:3028. https://doi.org/10.3390/APP14073028.

[15] Zhang Z, Zhang Y, Zhu P. Flexural behavior of precast RC deck panels with cast-in-place UHPFRC connection. Coatings 2022:12. https://doi.org/10.3390/coatings12081183.
[16] Vecchio FJ, Collins MP. The modified compression-field theory for reinforced concrete elements subjected to shear. Acids J Proc 1986;83:219–31. https://doi.org/10.14359/10416.
[17] Selby RG, Vecchio FJ. A constitutive model for analysis of reinforced concrete solids. Can J Civ Eng 1997;24:460–70. https://doi.org/10.1139/L96-135/ASSET/L96-135.FP.PNG_V03.
[18] Hordijk D.A. Local approach to fatigue of concrete. PhD Thesis, Delft University of Technology, 1991.
[19] Fédération Internationale du Béton (fib). fib Model Code for Concrete Structures 2010. vol. 1–2. Lausanne, Switzerland: Ernst & Sohn - fédération internationale du béton, Bulletin 65; 2012.
[20] Feenstra P.H. Computational aspects of biaxial stress in plain and reinforced concrete. PhD Thesis, Delft University of Technology: Civil Engineering and Geosciences, 1993.
[21] Nakamura H, Higai T. Compressive fracture energy and fracture zone length of concrete. In: Shing PB, Tanabe T, editors. Modeling of Inelastic Behavior of RC Structures under Seismic Loads. ASCE; 2001. p. 471–87.
[22] Fehling E, Schmidt M, Walraven JC, Leutbecher T, Fröhlich S. Ultra-high performance concrete UHPC: fundamentals, design, examples. Berlim Ernst Sohn 2014.
[23] Thorenfeldt E, Tomaszewicz A, Jensen J. Mechanical properties of high-strength concrete and applications in design. Norway: Stavanger, TAPIR TRONDHEIM NORWAY; 1987. p. 149–59. Proceedings of the Symposium Utilization of High Strength Concrete.
[24] Gao XL, Shen SY, Wan Y, Qin SW. Experimental study on bond behavior of steel bar embedded in thin UHPC. J Build Eng 2024;86:108865. https://doi.org/10.1016/J.JOBE.2024.108865.
[25] Pan R, Zou J, Liao P, Dong S, Deng J. Effects of fiber content and concrete cover on the local bond behavior of helically ribbed GFRP bar and UHPC. J Build Eng 2023;80:107939. https://doi.org/10.1016/J.JOBE.2023.107939.
[26] Soliman AA, Heard WF, Williams BA, Ranade R. Effects of the tensile properties of UHPC on the bond behavior. Constr Build Mater 2023;392:131990. https://doi.org/10.1016/J.CONBUILDMAT.2023.131990.
[27] Deng E-F, Zhang Z, Zhang C-X, Tang Y, Wang W, Du Z-J, et al. Experimental study on flexural behavior of UHPC wet joint in prefabricated multi-girder bridge. Eng Struct 2023;275:115314. https://doi.org/10.1016/j.engstruct.2022.115314.
[28] DIANA FEA. DIANA Finite Element Analysis User's Manual Release. 2023.
[29] Prado LP. Estudo da interface do concreto pré-moldado e concreto de altíssimo desempenho reforçado com fibras. Univ De São Paulo 2020. https://doi.org/10.11606/T.18.2020.tde-02052023-151717.
[30] AASHTO. AASHTO LRFD Bridge Design Specifications. 8th ed. Washington D.C.: American Association of State Highway and Transportation Officials (AASHTO); 2017.
[31] Graybeal B. Bond behavior of reinforcing steel in ultra-high-performance concrete. Washington, DC: 2014.
[32] Guo W, Fan W, Shao X, Shen D, Chen B. Constitutive model of ultra-high-performance fiber-reinforced concrete for low-velocity impact simulations. Compos Struct 2018;185:307–26. https://doi.org/10.1016/J.COMPSTRUCT.2017.11.022.
[33] Huang D, Nie X, Zeng J, Jiang Y. Experimental and numerical analysis on flexural behavior of improved U-bar joint details for accelerated bridge construction. Eng Struct 2023:289. https://doi.org/10.1016/j.engstruct.2023.116328.